UNIVERSITY OF CALIFORNIA SAN DIEGO

Functional Correlates of Adult Hippocampal Neurogenesis & Sensitivity of Hippocampal Neural Progenitor Cells to rAAV-induced Cell-death

A dissertation submitted in partial satisfaction
of the requirements for the degree Doctor of Philosophy

in

Neurosciences
with a Specialization in Computational Neurosciences

by

Stephen Thomas Johnston

Committee in charge:

Professor Fred Gage, Chair
Professor Andrea Chiba, Co-chair
Professor Edward Callaway
Professor Pascal Gagneux
Professor Byungkook Lim

2019

The Dissertation of Stephen Thomas Johnston is approved, and it is acceptable in quality and form for publication on microfilm and electronically:

_____

_____

_____

_____
Co-chair

_____
Chair

University of California San Diego

2019

DEDICATION

To the community of people who have provided me with an education greater than facts. You cannot know the small but profound ways you have all contributed to my life, know I am so grateful.

To the people who supported and inspired me most, my family—my dad, my sister, my mom, my nephew, my niece, Amanda, Cheyenne.

EPIGRAPH

“It is in the admission of ignorance and the admission of uncertainty that there is a hope for the continuous motion of human beings in some direction that doesn't get confined, permanently blocked…. I don't feel frightened by not knowing things, by being lost in the mysterious universe.... It doesn't frighten me.”

"There is great pleasure to be had in doing things that are crazy... things that *other people* think are crazy."

-Richard Feynman

“It’s not the mean that’s interesting, the variation is.”

-Fred “Rusty” Gage

TABLE OF CONTENTS

LIST OF FIGURES

LIST OF TABLES

ACKNOWLEDGEMENTS

I would like to acknowledge the members of the Gage lab for their support and tolerance: of whom it has been an honor to count as colleagues, teachers, and compatriots, and without whom I would have achieved far less. I would like to thank: Foremost, my advisor, Fred "Rusty" Gage, for tremendous support when life throws you an unexpected post-developmental structural plasticity event and being aware of the signs before I was; The greater Salk and UCSD communities – particularly the members across the Laboratory of Genetics and Callaway labs, and the Center for Academic Research & Training in Anthropogeny "CARTA" – whom all ensured I never had to look too far to find a brilliant person to get advice from or a brilliant but necessary distraction to remember there was a world outside and to look up from my bench or microscope; The UCSD Neurosciences Graduate Program–in particularly my cohort & affiliated stragglers, and the program administrators– for intellectual, social, and bureaucratic support that ensured my success. The students and technicians I have mentored – who made my science better and more fulfilling. The mice, who made this work possible.

I would like to acknowledge generous funding from the Dan and Martina Lewis Biophotonics Fellows Program and James S. McDonnell Foundation.

Introduction, Figure 0.1, is adaptation of the material as it appears in: Poo MM, Pignatelli M, Ryan TJ, Tonegawa S, Bonhoeffer T, Martin KC, Rudenko A, Tsai LH, Tsien RW, Fishell G, Mullins C, Gonçalves JT, Shtrahman M, Johnston ST, Gage FH, Dan Y, Long L, Buzsáki G, Stevens C. (2016) What is memory? The present state of the engram. *BMC Biology*, 14:40. The dissertation author was a contributing author for this figure.

Chapter 1, in full, is a reprint of the material as it appears in: Johnston ST, Shtrahman M, Parylak S, Gonçalves JT, Gage FH. (2016) Paradox of pattern separation and adult neurogenesis:

A dual role for new neurons balancing memory resolution and robustness. *Neurobiology of Learning and Memory,* 129 60-68, https://doi.org/10.1016/j.nlm.2015.10.013 . The dissertation author was the primary investigator and author of this paper.

Chapter 2, in full, is coauthored unpublished material: Johnston ST, Parylak SL, Kim S, Mac N, Lim CK, Gallina IS, Bloyd CW, Alex Newberry Saavedra CD, Ondřej Novák, Gonçalves JT, Gage FH, Shtrahman M. AAV induced cell-death of Neural Progenitor Cells in the Dentate Gyrus. The dissertation author was the primary investigator and author of this paper.

VITA

2008	Bachelor of Science, Physics – Oklahoma State University
	Bachelor of Science, Mathematics – Oklahoma State University
	Bachelor of Science, Political Science – Oklahoma State University Minor: History
2010-2012	Research Technician – Washington State University
2014-2016	Teaching Assistant – University of California San Diego
2019	Doctor of Philosophy – University of California San Diego Specialization: Computational Neuroscience Specialization: Anthropogeny

PUBLICATIONS

Mansour AA, Gonçalves JT, Bloyd CW, Li H, Fernandes S, Quang D, **Johnston S**, Parylak SL, Jin X, Gage FH. (2018) An in vivo model of functional and vascularized human brain organoids. *Nat Biotechnol* 36, 432–441.

Johnston ST, Shtrahman M, Parylak S, Gonçalves JT, and Gage FH. (2016) Paradox of pattern separation and adult neurogenesis: A dual role for new neurons balancing memory resolution and robustness. *Neurobiol Learn Mem* 129, 60-68.

Poo MM, Pignatelli MR, Tomás J, Tonegawa S, Bonhoeffer T, Martin KC, Rudenko A, Tsai LH, Tsien RW, Fishell G, Mullins C, Gonçalves JT, Shtrahman S, **Johnston ST**, Gage FH, Dan Y, Long J, Buzsáki G, Stevens C. (2016) What is memory? The present state of the engram. *BMC Biol* 14: 40.

Gonçalves JT, Bloyd CW, Shtrahman M, **Johnston ST**, Schafer ST, Parylak SL, Tran T, Chang T, and Gage FH. (2016) In vivo imaging of dendritic pruning in dentate granule cells. *Nat Neurosci* 19, 788–791.

Han J, Kim HJ, Schafer ST, Paquola A, Clemenson GD, Toda T, Oh J, Pankonin AR, Lee BS, **Johnston ST**, Sarkar A , Denli AM, Gage FH. (2016) Functional Implications of miR-19 in the Migration of Newborn Neurons in the Adult Brain. *Neuron* 91, 79–89.

Gallaher ZR, **Johnston ST**, and Czaja, K. (2014) Neural proliferation in the dorsal root ganglia of the adult rat following capsaicin-induced neuronal death. *J Comp Neurol* 522, 3295–3307.

Johnston ST, Gallaher Z, and Czaja K. (2012) Exogenous reference gene normalization for real-time reverse transcription-polymerase chain reaction analysis under dynamic endogenous transcription. *Neural Regen Res* 7, 1064–1072.

ABSTRACT OF THE DISSERTATION

Functional Correlates of Adult Hippocampla Neurogenesis
& Sensitivity of Hippocampal Neural Progenitor Cells to rAAV-induced Cell-death

by

Stephen Thomas Johnston

Doctor of Philosophy in Neurosciences
with Specialization in Computational Neuroscience

University of California San Diego, 2019

Professor Fred H. Gage, Chair
Professor Andrea Chiba, Co-chair

The elegantly delineated anatomy of the hippocampus has long served as a substrate for theories of memory formation and recall. Principally, the Dentate Gyrus (DG) has been proposed to be important in the encoding and formation of new memories through a process known as pattern separation, while downstream CA3 has been proposed to play a role in memory recall through a process known as pattern completion. *In vivo* optical methods have provided access to study computation within the DG and the activity of dentate granule cells (DGCs) has been associated with hippocampus-dependent behavioral pattern separation and pattern completion. Increasing evidence supports the idea that a rare population of immature adult-born DGCs (abDGCs) 4-6 weeks of age support pattern-separation in the DG by enhancing feedback

inhibition onto mature DGCs. These studies rely almost exclusively on recominant Adeno-associated Virus (rAAV) for transgene delivery, however the toxic effects of rAAV on this circuit were not been assessed.

Herein, we demonstrate that neural progenitor cells (NPCs) and immature DGCs within the adult murine hippocampus are particularly sensitive to rAAV induced cell-death. Cell loss is dose-dependent and nearly complete at experimentally relevant viral titers. rAAV induced cell-death is rapid and persistent, with loss of BrdU labeled cells within 18 hours post-injection and no evidence of recovery of adult neurogenesis when assessed at 3 months post-injection. The remaining mature DGCs appear hyperactive 4 weeks post-injection based on immediate early gene expression, consistent with previous studies investigating the effects of attenuating adult neurogenesis. This rAAV-induced toxicity is intrinsic to the rAAV viral vector. Finally, efficient transduction of the DG is achieved by injection of rAAV2-retro serotyped virus into CA3 and permits *in vivo* 2-photon calcium imaging of dentate activity while leaving adult neurogenesis intact. Using this method we demonstrate functional changes to mature DGC activity 2-weeks following abDGC ablation using rAAV. These findings expand on recent reports implicating rAAV linked toxicity in stem cells and other cell types and suggests future work using rAAV in the DG should be carefully evaluated.

INTRODUCTION

For nearly 50 years theorists have attempted to understand how computations underlying memory formation and retrieval arise from the elegantly delineated anatomy of the hippocampus (Marr, 1971; Treves and Rolls, 1994). However, a clear proof of these theories has remained elusive. Memory involves the complex interplay between forming representations of new events and generalizing those representations to similar experiences. Distinct but similar memories must be discriminated—for example, being able to find your car at work despite parking in a different spot each day. At the same time, memories must be employed to generalize across learning experiences, despite distinct differences, to permit effective learning—for example, knowing how to follow a well-known route despite differences in environmental or other conditions. The interplay between forming distinct memories and generalizing events is conceptualized to involve two separate processes: pattern separation and pattern completion, respectively.

As the gateway to the hippocampus, the dentate gyrus (DG) plays a crucial role in hippocampal function. With approximately 5-10 times more neurons in the DG than projection neurons in upstream entorhinal cortex, neural representations are massively expanded into the DG, before being condensed again into downstream CA3. This process is thought to subserve memory formation by providing the representational space for distinct non-overlapping memory representations through the process of pattern separation. The hippocampus is all the more unique in that it is home to one of two pools of neural stem cells that give rise to functional neurons throughout the adult life adult mammals.

Adult-born DGCs (abDGCs) undergo a lengthy process of morphological and physiological maturation before they fully integrate into the local hippocampal network (Espósito et al., 2005). Each immature DGC enters a period of enhanced plasticity approximately

4 to 6 weeks after it is born. These immature DGCs exhibit greater excitability (Schmidt-Hieber et al., 2004), receive less inhibition from local interneurons (Li et al., 2012), are more broadly tuned to input stimuli (Marin-Burgin et al., 2012), and exhibit greater synaptic plasticity (Ge et al., 2007) than mature cells. Therefore, immature abDGCs are thought to uniquely contribute to learning and memory through their own activity and by modulating population activity within the DG (Fig. 0.1; Gonçalves et al., 2016; Johnston et al., 2016; Sahay et al., 2011)

Immature adult-born neurons improve pattern-separation in the DG by enhancing feedback inhibition. Two events are encoded in separate but partially overlapping populations of activated DGCs in the DG (red and green, with overlap in yellow). DGCs receive strong inhibitory inputs from interneurons (purple) in the hilus and sub-granular zone. It is hypothesized that hyperactive immature adult-born DGCs (blue) drive these interneurons, enhancing feedback inhibition from the hilus, which results in decreased overlap of activated DGCs and output to CA3, thereby improving pattern separation

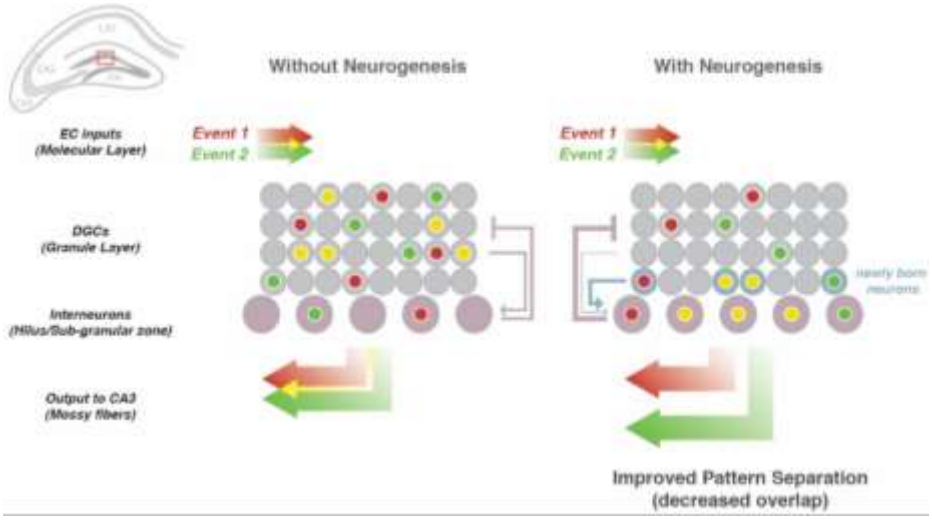

Fig. 0.1. Immature adult-born neurons improve pattern-separation in the DG by enhancing feedback inhibition. Two events are encoded in separate but partially overlapping populations of activated DGCs in the DG (red and green, with overlap in yellow). DGCs receive strong inhibitory inputs from interneurons (purple) in the hilus and sub-granular zone. It is hypothesized that hyperactive immature adult-born DGCs (blue) drive these interneurons, enhancing feedback inhibition from the hilus, which results in decreased overlap of activated DGCs and output to CA3, thereby improving pattern separation. Adapted from Gonçalves et al. in Poo et al.

abDGCs have been difficult to study. First, adult-born DGCs are a relatively heterogeneous population of cells – undergoing a unique maturation process, with their properties varying over time. Second, abDGCs are relatively rare and difficult to access, more than 2mm inside the mouse brain. Third, these cells are sensitive to environmental stimuli with proliferation, survival, and dendritic outgrowth regulated *in vivo* by experience, stress, and systemic and local inflammation (Bayer and Altman, 1974; Ge et al., 2006; Gonçalves et al., 2016b; Kempermann, 2006; Song et al., 2013; Vivar et al.). Therefore ex vivo and post-mortem studies do not fully represent the state of the complex contributions of this population of cells.

Using i*n vivo* optical methods, work begun in this lab as an extension of methods developed for this dissertation, and later expanded by other labs, the *in* vivo proliferation and development of abDGCs was recently structurally resolved (Gonçalves et al., 2016b; Pilz et al., 2018). Preliminary work has also permitted dentate and hilar activity to be quantified (Anacker et al., 2018; Danielson et al., 2016, 2017; Hayashi et al., 2017; Kirschen et al., 2017; Pilz et al., 2018). These functional studies represented a step forward in providing access to disambiguate an otherwise heterogeneous population of cells (Danielson et al., 2017; GoodSmith et al., 2017; Leutgeb et al., 2007; Nakazawa, 2017; Senzai and Buzsáki, 2017). Crucially, these studies rely almost exclusively on rAAV for transgene delivery, however the toxic effects of rAAV on this circuit have not been previously assessed (Danielson et al., 2016; Hayashi et al., 2017; Liu et al., 2014; Pilz et al., 2016; Ramirez et al., 2013; Swiech et al., 2015; Zhu et al., 2014).

The widespread use rAAV in human and animals studies endorsed the long held belief of the relative lack of pathogenicity of AAV which has made it ideal for transgene delivery. However, three recent reports have demonstrated AAV-induced toxicity in stem cells and other

cell types (Hirsch, Hinderer et al., 2018; Hordeaux et al., 2018). Motivated by our own early efforts to study the role of adult neurogenesis in DG function and hippocampus-dependent behavior, we discovered that neural progenitor cells (NPCs) in the DG are highly sensitive to rAAV-induced death at experimentally relevant titers.

We demonstrate that NPCs and immature dentate granule cells (DGCs) within the adult mouse hippocampus are particularly sensitive to rAAV-induced cell-death. This cell loss is dose-dependent and nearly complete at experimentally relevant viral titers. rAAV induced cell-death is rapid and persistent, with loss of BrdU labeled cells and Tbr2+ intermediate progenitors cells within 18 hours post-injection and no evidence of recovery of adult neurogenesis when assessed at 3 months post-injection. The remaining mature DGCs appear hyperactive 4 weeks post-injection based on immediate early gene expression, consistent with previous studies investigating the effects of attenuating adult neurogenesis. *In vitro* application of AAV or electroporation of AAV2 inverted terminal repeats (ITRs) is sufficient to induce cell death; independent of local inflammation *in vivo.*

We further demonstrate that efficient transduction of the dentate gyrus (DG)—without ablating adult neurogenesis—can be achieved by injection of rAAV2-retro serotyped virus into CA3. rAAV2-retro results in efficient retrograde labeling of mature DGCs and permits *in vivo* 2-photon calcium imaging of DG activity while leaving adult neurogenesis intact. This method sets the stage for future work which will permit the manipulation and visualization of DGCs *in vivo* without disrupting the contribution of abDGCs to DG and hippocampal development, activity and function.

REFERENCES

Bayer, S.A., and Altman, J. (1974). Hippocampal development in the rat: cytogenesis and morphogenesis examined with autoradiography and low-level X-irradiation. J. Comp. Neurol. *158*, 55–79.

Espósito, M.S., Piatti, V.C., Laplagne, D.A., Morgenstern, N.A., Ferrari, C.C., Pitossi, F.J., and Schinder, A.F. (2005). Neuronal Differentiation in the Adult Hippocampus Recapitulates Embryonic Development. J. Neurosci. *25*, 10074–10086.

Ge, S., Goh, E.L.K., Sailor, K.A., Kitabatake, Y., Ming, G., and Song, H. (2006). GABA regulates synaptic integration of newly generated neurons in the adult brain. Nature *439*, 589.

Ge, S., Yang, C., Hsu, K., Ming, G., and Song, H. (2007). A Critical Period for Enhanced Synaptic Plasticity in Newly Generated Neurons of the Adult Brain. Neuron *54*, 559–566.

Gonçalves, J.T., Schafer, S.T., and Gage, F.H. (2016a). Adult Neurogenesis in the Hippocampus: From Stem Cells to Behavior. Cell *167*, 897–914.

Gonçalves, J.T., Bloyd, C.W., Shtrahman, M., Johnston, S.T., Schafer, S.T., Parylak, S.L., Tran, T., Chang, T., and Gage, F.H. (2016b). In vivo imaging of dendritic pruning in dentate granule cells. Nat. Neurosci. *19*, 788–791.

Johnston, S.T., Shtrahman, M., Parylak, S., Gonçalves, J.T., and Gage, F.H. (2016). Paradox of pattern separation and adult neurogenesis: A dual role for new neurons balancing memory resolution and robustness. Neurobiol. Learn. Mem. *129*, 60–68.

Kempermann, G. (2006). Adult Neurogenesis: Stem Cells and Neuronal Development in the Adult Brain (Oxford University Press).

Li, Y., Aimone, J.B., Xu, X., Callaway, E.M., and Gage, F.H. (2012). Development of GABAergic inputs controls the contribution of maturing neurons to the adult hippocampal network. Proc. Natl. Acad. Sci. *109*, 4290–4295.

Marin-Burgin, A., Mongiat, L.A., Pardi, M.B., and Schinder, A.F. (2012). Unique Processing During a Period of High Excitation/Inhibition Balance in Adult-Born Neurons. Science *335*, 1238–1242.

Marr, D. (1971). Simple Memory: A Theory for Archicortex. Philos. Trans. R. Soc. Lond. B Biol. Sci. *262*, 23–81.

Sahay, A., Wilson, D.A., and Hen, R. (2011). Pattern Separation: A Common Function for New Neurons in Hippocampus and Olfactory Bulb. Neuron *70*, 582–588.

Schmidt-Hieber, C., Jonas, P., and Bischofberger, J. (2004). Enhanced synaptic plasticity in newly generated granule cells of the adult hippocampus. Nature *429*, 184–187.

Song, J., Sun, J., Moss, J., Wen, Z., Sun, G.J., Hsu, D., Zhong, C., Davoudi, H., Christian, K.M., Toni, N., Ming, G., and Song, H. (2013). Parvalbumin interneurons mediate neuronal circuitry–neurogenesis coupling in the adult hippocampus. Nat. Neurosci. *16*, 1728–1730.

Treves, A., and Rolls, E.T. (1994). Computational analysis of the role of the hippocampus in memory. Hippocampus *4*, 374–391.

Vivar, C., Peterson, B.D., and van Praag, H. Running rewires the neuronal network of adult-born dentate granule cells. NeuroImage.

Introduction, Fig. 0.1, is adaptation of the material as it appears in: Poo MM, Pignatelli M, Ryan TJ, Tonegawa S, Bonhoeffer T, Martin KC, Rudenko A, Tsai LH, Tsien RW, Fishell G, Mullins C, Gonçalves JT, Shtrahman M, Johnston ST, Gage FH, Dan Y, Long L, Buzsáki G, Stevens C. (2016) What is memory? The present state of the engram. *BMC Biology*, 14:40. The dissertation author was a contributing author for this figure.

CHAPTER 1: Paradox of Pattern Separation and Adult Neurogenesis: A Dual Role for New Neurons Balancing Memory Resolution and Robustness

Contents lists available at ScienceDirect

Neurobiology of Learning and Memory

journal homepage: www.elsevier.com/locate/ynlme

Review

Paradox of pattern separation and adult neurogenesis: A dual role for new neurons balancing memory resolution and robustness

Stephen T. Johnston, Matthew Shtrahman, Sarah Parylak, J. Tiago Gonçalves, Fred H. Gage *

Laboratory of Genetics, Salk Institute for Biological Studies, La Jolla, CA 92037, United States

ARTICLE INFO

Article history:
Received 16 July 2015
Revised 22 October 2015
Accepted 27 October 2015
Available online 6 November 2015

Keywords:
Dentate gyrus
Adult neurogenesis
Pattern separation
Pattern completion
Memory resolution
Memory robustness

ABSTRACT

Hippocampal adult neurogenesis is thought to subserve pattern separation, the process by which similar patterns of neuronal inputs are transformed into distinct neuronal representations, permitting the discrimination of highly similar stimuli in hippocampus-dependent tasks. However, the mechanism by which immature adult-born dentate granule neurons cells (abDGCs) perform this function remains unknown. Two theories of abDGC function, one by which abDGCs modulate and sparsify activity in the dentate gyrus and one by which abDGCs act as autonomous coding units, are generally suggested to be mutually exclusive. This review suggests that these two mechanisms work in tandem to dynamically regulate memory resolution while avoiding memory interference and maintaining memory robustness.

1. Introduction

The brain continuously simplifies and integrates sensory experiences in the context of prior memories to generate the perceptions through which we interact with the world. We perform this integration most vividly as we conjure previous memories and compare and contrast them to our current experience, as is the case with highly salient episodic memories. On the one hand, we are able to differentiate between similar experiences, such as today's lunch and yesterday's. On the other hand, as with Proust's episode of the madeleine, an incomplete stimulus such as a single bite of a familiar meal allows us to mentally jump to another time and place, unleashing a flood of memories reconstructed from only part of the original experience. In reality, however, the brain is perpetually engaged in a parallel competition between new, discrete memory formation and generalization across similar experiences. Adult neurogenesis, the process by which new neurons are added to the dentate gyrus (DG) of the hippocampus (HC) throughout the life of an individual, is critical to the encoding and retrieval of these memories, particularly when the experiences are highly similar. This review focuses on the contribution of adult neurogenesis to the process of learning and memory and its possible role in permitting the hippocampus to dynamically and continuously optimize memory resolution and robustness.

2. Pattern separation by the dentate gyrus

The balance between discrimination and generalization is thought to be subserved by two competing processes: (1) *pattern separation*, the process by which distinct, but often overlapping or highly similar patterns of neuronal inputs are transformed into distinct neuronal representations, thereby allowing for the accurate formation of a new memory without interference from other memory representations, and (2) *pattern completion*, the process by which a full memory representation is evoked from a partial set of inputs that are often a subset of a similar but distinct memory or experience (Figs. 1i and 2i–iii). These computations are performed not through individual neurons but through the concerted activity of networks of neurons. Growing evidence indicates that the functionally distinct circuitries of each subregion of the HC differentially and simultaneously employ different balances of these processes to contribute their own degree of discrimination to hippocampal memory formation and retrieval (Fig. 1ii).

First among these subregions, the DG has been proposed as a "gateway" to the HC. Receiving non-spatial contextual information from the lateral entorhinal cortex (LEC) and metric spatial information from the medial entorhinal cortex (MEC), the DG compresses and conjunctively encodes multimodal sensory and spatial representations about the environment that are then passed on to the rest of the HC for processing (Hunsaker, Mooy, Swift, & Kesner, 2007; McClelland, McNaughton, & O'Reilly, 1995). These representations from the EC are transformed into sparse representations in

* Corresponding author.
E-mail address: gage@salk.edu (F.H. Gage).

http://dx.doi.org/10.1016/j.nlm.2015.10.013
1074-7427/

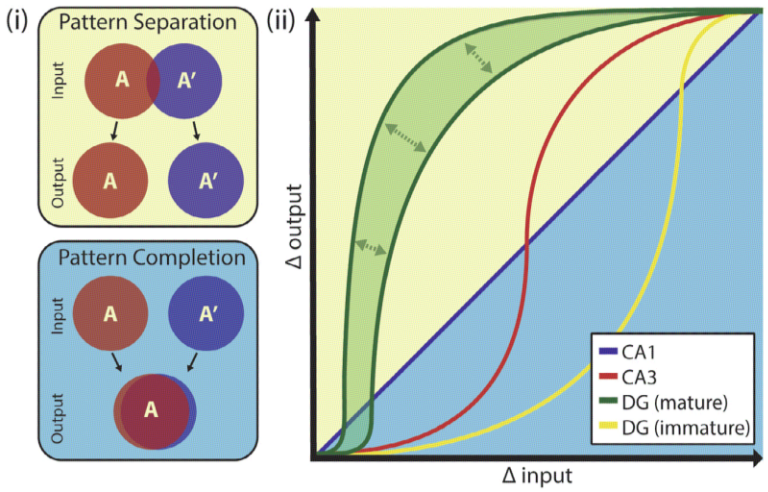

Fig. 1. Neurogenesis dynamically regulates pattern separation. (i) A schematic representation of pattern separation and completion. Pattern separation can be thought of as the process by which distinct, but often overlapping or highly similar patterns of neuronal inputs (A and A′) are transformed into more distinct neuronal representations, shown here as a decrease in overlap between A and A′. Pattern completion can be thought of as the process by which a full memory representation is reconstructed from a similar representation of partially overlapping inputs, represented here as A′ becoming more similar to A (Fig. 2ii), or from a subset of the inputs (Fig. 2iii). (ii) Nonlinear transformations for DG and CA3 by which each region initially pattern completes for nearby inputs but pattern separates for larger differences in inputs, each component contributing a different level of discrimination as Δ input is transformed into Δ output. The diagonal line represents equal differences in input and output, i.e., Δ input = Δ output. The region above the line represents conditions in which inputs are made more dissimilar (i.e., pattern separation), and the region below the line represents conditions in which inputs are made more similar (i.e., pattern completion). On the individual cell level, immature abDGCs integrate patterns across a wide range of inputs, resulting in pattern completion, with the ultimate result of dynamically modulating pattern separation in mature abDGCs on the network level. Adapted from Yassa & Stark, 2011.

the DG, as representations are expanded onto downstream dentate granule neurons (DGCs) that are 5–10 times more numerous than their upstream EC pyramidal neuron counterparts. This marked expansion of the neuronal population, extremely low inter-region connectivity (i.e., each DGC synapses on ~10 CA3 pyramidal neurons, two to three orders of magnitude less than the number of EC-DG or EC-CA3 synapses each EC pyramidal neuron makes; Amaral, Ishizuka, & Claiborne, 1990; Mulders, West, & Slomianka, 1997; Schmidt, Marrone, & Markus, 2012), and low intrinsic activity of the DGC population (Gothard, Hoffman, Battaglia, & McNaughton, 2001; Jung & McNaughton, 1993; O'Reilly & McClelland, 1994) are believed to allow for the formation of a sparse, distributed code. Traditional 'connectionist' or Hopfield-like network models suggest that the DG uses this sparse coding to increase the number of available representations by minimizing overlap between patterns of activity (Amit, Gutfreund, & Sompolinsky, 1987; Marr, 1971; McClelland et al., 1995; O'Reilly & McClelland, 1994; Treves & Rolls, 1994). Noting that where representations are not orthogonalized the system rapidly breaks down due to catastrophic interference (McClelland et al., 1995; McCloskey & Cohen, 1989), others have expanded these models to include an "error checking" function in CA3-DG feedback to avoid interference (Lisman, 1999; Rennó-Costa, Lisman, & Verschure, 2010).

While these connectionist models generally do not make strict distinctions between behavioral phases of encoding and recall, it has been suggested that, during memory formation, decorrelated patterns of activity undergo further enhancement before being transferred with relatively high fidelity from the DG to the CA3 through the mossy fibers to promote memory formation (Henze, Wittner, & Buzsáki, 2002; Urban, Henze, & Barrionuevo, 2001). In parallel, the relatively weaker but more active EC-CA3 perforant path connection provides direct input from the EC to promote memory recall (Lassalle, Bataille, & Halley, 2000; Lee & Kesner, 2004). It has therefore been proposed that, while the major functions of the HC are to encode and discriminate spatial and contextual events from one another, the sensitivity of the DG to small changes in input makes it particularly important when encoding highly similar stimuli and less important in promoting recall (Kesner, 2007; Lee & Kesner, 2004; though see a dissenting opinion in Nakashiba et al., 2012). It has been noted, however, that making a distinction between encoding and retrieval phases may prove difficult as learning and recall are fundamentally intertwined (Kesner, 2007; Rolls & Kesner, 2006).

These models can be conceptualized as a competition between the pattern separation of memory formation and pattern completion of memory recall (Fig. 1). A useful visualization for conceptualizing these attractor networks is a phase space diagram (See information box "Attractor Networks of Memory" and Fig. 2). Inputs, even if closely associated in phase space such as those on opposite sides of a "hill," can settle into different output states and be thought of as pattern separation (Fig. 2i). Inputs that settle into the same output state can be thought of as pattern completion (Fig. 2ii and iii). In the models above, the CA3 initially pattern completes, as recurrent activity leads similar inputs to recruit the same population of output neurons through attractor formation and thereby allows for the recall of memories (Fig. 1ii). However, the CA3 pattern separates if incoming inputs are similar but sufficiently distinct, represented here as a smooth phase space of long hills and troughs (Fig. 3i). On the other hand, the DG rapidly pattern separates as similar inputs are mapped onto distinct populations of output neurons, represented as a rougher, discrete phase space of sharp hills and valleys (Fig. 3ii), where only nearly identical inputs result in the same output (i.e., limited pattern completion). The DG contributes resolution for highly similar stimuli because it discriminates between fine details; however, the DG is

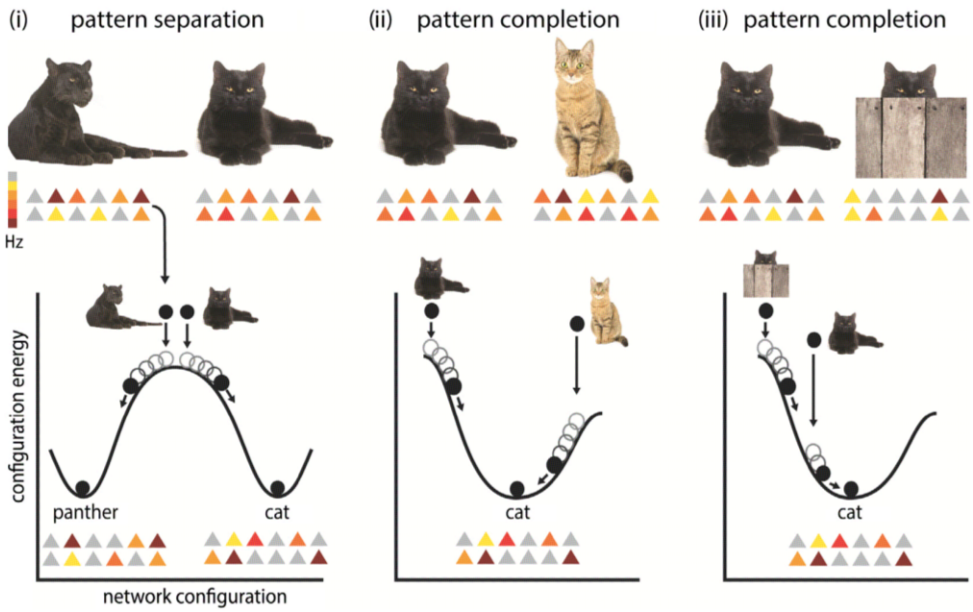

Fig. 2. Hippocampal pattern separation and pattern completion conceptualized in phase space. (i) Schematic of pattern separation where similar but distinct experiences, depicted by a black panther and a black cat, are encoded by similar patterns of neuronal network activity (network configuration). The network is optimized, presumably through synaptic plasticity during learning, such that neighboring input states separate and flow downhill to different low energy attractor states that are far apart in network configuration or "phase" space. These stable states are thought to code for percepts or other behaviorally relevant output of the network, such as "panther" or "cat". (ii) The energy landscape of phase space is complex and can also be shaped to encourage pattern completion, where distinct experiences are lumped together and generalized through convergence of their resulting network activity patterns. (iii) Alternatively, the same process can facilitate another form of pattern completion, where a full memory representation is evoked from a partial set of inputs.

likely unable to discriminate differences between small changes in input and large changes in input (Fig. 1ii). Both differences are already entirely orthogonalized (i.e., increasing the change in input does not increase the change in output), and the resulting overlap would not be greater than chance (Deng, Mayford, & Gage, 2013).

Behavioral support for the role of the DG as a pattern separator of highly similar stimuli first came in the form of lesion studies in which ablation or blockage of plasticity in the DG resulted in impaired discrimination of similar spatial and contextual information (Gilbert, Kesner, & Lee, 2001; Goodrich-Hunsaker, Hunsaker, & Kesner, 2008; McHugh et al., 2007; Nakashiba et al., 2012; Saxe et al., 2007). The mechanism by which the DG actually performs this function, however, remains unclear. In vivo electrophysiological recordings suggest that, while small changes in environmental cues induce changes in the rate coding of DGCs, they do not result in the decorrelation of the population of active cells that the connectionist models above are predicated upon (Alme et al., 2010; Leutgeb, Leutgeb, Moser, & Moser, 2007). However, in agreement with the above computational theories, results from our lab and others employing immediate early gene (IEG) quantification as an alternate method of looking at entire populations of cells in the DG suggest that the DG rapidly decorrelates representations into distinct populations of DGCs with limited overlap to represent small changes in environmental inputs (Chawla et al., 2005; Deng et al., 2013). The relative strengths and weaknesses of these methods may make them inherently better suited to detect changes in rate or population coding. Electrophysiological recordings provide temporal resolution at the level of individual neuronal spikes, which can be directly correlated to a behavior as it is being performed. However, it is likely that all but the most active neurons in the dentate are recorded. Further, they lack the spatial resolution and cellular identification required to demonstrate population coding of the sparsely activated DG. In contrast, IEG methods provide spatial resolution and cellular identification. However, they lack temporal resolution, allowing only a single time point to be investigated, and minimal activity required which results in their induction remains unknown (Schoenenberger, Gerosa, & Oertner, 2009), preventing IEGs from being used to investigate rate encoding. IEGs also likely underreport total neuronal activity but may be less prone to neuronal noise. Despite these limitations, the literature still appears to be in conflict between rate and population encoding in the DG. It has been suggested that this conflict can be resolved by dividing the DG into two distinct populations (Alme et al., 2010; Deng et al., 2013; Neunuebel & Knierim, 2012; Piatti, Ewell, & Leutgeb, 2013). The first population is composed of the majority of DGCs, is sparsely activated, and is engaged in population coding; representations including these cells rapidly orthogonalize in response to small changes in environmental inputs and are missed by electrophysiological recordings. This population is likely mature DGCs. The second population of DGCs is more active, with signals frequent enough to be recorded in vivo, and does not rapidly orthogonalize. This second population of broadly tuned DGCs is proposed to represent hyperactive, immature adult-born dentate granule cells (abDGCs), and it may be missed by IEG studies (Huckleberry et al., 2015; Jessberger & Kempermann, 2003; Snyder, Glover, Sanzone, Kamhi, & Cameron, 2009; Snyder, Choe, et al., 2009). [An alternative explanation may be that, like CA1 and CA3, the DG uses alternate encoding methods to represent different types of information (Leutgeb, Leutgeb, Barnes, et al., 2005); however, these discrepancies may also be due to differences in behavioral protocols (Leutgeb, Leutgeb, Treves, et al., 2005; Wills et al., 2005). Such transitions between population and rate coding have not been directly tested in the DG.]

Attractor Networks of Memory

The attractor neural network (Poucet & Save, 2005; Wills, Lever, Cacucci, Burgess, & O'Keefe, 2005) is a theoretical framework useful for understanding ensemble neural activity and building intuition about the much theorized processes of pattern separation and pattern completion. Adapted from statistical physics, the state of the network is represented as a location in an abstract multidimensional space that describes all the possible configurations of the network (Fig 2). This *N*-dimensional configuration or "phase" space is perhaps most easily conceptualized as being bound by *N* axes, each describing the firing rate for one of the *N* neurons within the network*. Each distinct combination of the *N* firing rates, or configuration, is represented by a unique point in phase space. Figs. 2 and 3 show schematics of this conceptualization in which each pattern of sensory stimuli or upstream neuronal activation results in a unique network state. However, while the initial state of the network is unique for a given set of inputs, the final state is not. Each of these configurations is assigned an energy describing the stability of the state of the network. Analogous to a ball rolling on a hilly landscape, the configuration of the network tends to flow toward local valleys that have lower energy. These stable network states exist in local energy minima and are thought to code for percepts or other behaviorally relevant representations of the network. Thus, depending on the roughness of the landscape, similar inputs eliciting network activity represented by nearby points in configuration space may (pattern completion, Fig. 2ii and iii) or may not (pattern separation, Fig. 2i) result in the same network representation. Presumably, the topology of the landscape, including the location of stable states and the roughness of their surroundings, is shaped through synaptic plasticity and other cellular and network processes in order to optimize computations relevant to the system (Fig. 3). As we describe below, it appears that the DG has been optimized to have a relatively rough landscape with a bias toward pattern separation, in which inputs that start off closely associated in configuration space are driven toward separate final states. In contrast, other areas of the HC, such as CA3, are smoother, facilitating pattern completion of similar upstream activity by driving similar inputs toward the same final state.

* In reality we do not know whether it is firing rate, spike timing, or other parameters that are truly relevant to the state of the network.

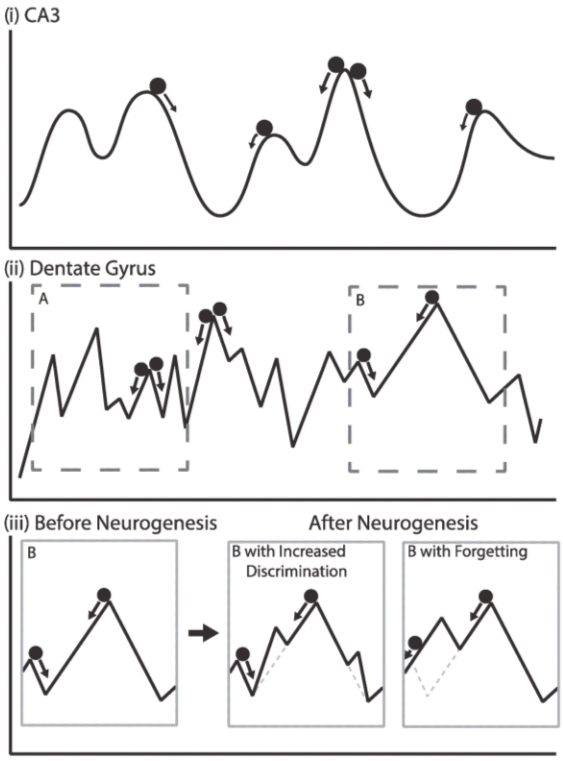

Fig. 3. Distinct roles for subfields within the hippocampal formation. Hippocampus-dependent memory formation and recall are constructed through a competition between *pattern completion*—driving similar inputs into the same attractor state—and *pattern separation*—driving similar inputs into distinct attractor states. (i) CA3 is represented as a smoother state space by which a large range of inputs leads to the same local minima, i.e., increased pattern completion. (ii) DG is represented as a rougher space with more discrete states. Small differences can lead to different local minima, i.e., increased pattern separation. Even within the DG, some of these spaces are smoother than others (A *vs.* B), permitting pattern completion at the cost of memory resolution (i.e., the fineness of discrete attractor states). (iii) Neurogenesis acts as an additional mechanism to increase resolution in these areas. A distributed code of overlapping mature DGCs sparsely encodes the input space into the output attractor space. Hyperexcitable immature DGCs, however, act as signal integrators to sample the state space and increase discrimination in low resolution (smooth) areas in an activity-dependent fashion by imposing "roughness" on the phase space, increasing the number of discrete states and adding local minima by acting as autonomous coding units and through disynaptic lateral inhibition. abDGCs may also increase rates of forgetting, conceptualized here as the replacement of one output state by another.

3. Neurogenesis is critical to pattern separation

Immature abDGCs undergo a critical period of increased excitability and enhanced plasticity (Espósito et al., 2005; Ge, Sailor, Ming, & Song, 2008; Ming & Song, 2011; Schmidt-Hieber, Jonas, & Bischofberger, 2004) as they begin to influence the activity of the local DG/hilar network and CA3. During this critical period, abDGCs have been shown to be behaviorally important for the encoding of new memories in the hippocampus (Dupret et al., 2008; Garthe, Behr, & Kempermann, 2009; Jessberger et al., 2009; Shors et al., 2001; Wojtowicz, Askew, & Winocur, 2008), with more recent studies demonstrating that, as animals undergo a variety of natural, genetic, and pharmacological manipulations of neurogenesis rates, their ability to discriminate spatial and contextual information is altered. This finding suggests that pattern separation within the DG is critically dependent upon adult neurogenesis.

Generally, when animals are subjected to decreases in neurogenesis, they are impaired in fine discrimination pattern separation tasks (Clelland et al., 2009; Clemenson et al., 2015; Nakashiba et al., 2012; Tronel et al., 2012), whereas increasing neurogenesis is sufficient to improve pattern separation (Creer, Romberg, Saksida, van Praag, & Bussey, 2010; Sahay, Scobie, et al., 2011). However, contrary to this simplification, increasing neurogenesis may also result in a deficit in discrimination for easier tasks, apparently as the animal over-generalizes a response (Clemenson et al., 2015). Surprisingly, this deficit is rescued, with animals with increased neurogenesis outperforming controls if a more difficult task is implemented (Clemenson et al., 2015). These results suggest a more complex story in which not only the cognitive strategies of

animals is altered by experience-induced increases in neurogenesis but also HC connectivity, in which abDGCs have different inputs depending on the environment in which they matured (Bergami et al., 2015; Deshpande et al., 2013).

Techniques for altering neurogenesis rates do vary in magnitude and temporal selectivity, with some knockdown strategies such as focal x-irradiation producing near-complete and permanent loss of abDGCs (Mizumatsu et al., 2003; Monje, Mizumatsu, Fike, & Palmer, 2002) and others such as inducible transgenic systems that promote apoptosis sparing some of the newborn population (Deng, Saxe, Gallina, & Gage, 2009; Tronel et al., 2012) and allowing progenitor cell proliferation to rebound after the end of treatment (Deng et al., 2009). Genetic strategies are gaining popularity, but care must be taken to restrict expression to the desired population to obtain comparable results [Saxe et al., 2007 for example, uses a GFAP promoter with the hope of ablating radial stem cells which give rise to abDGCs, however this method is likely to have broad effects throughout the brain given extensive expression of GFAP in glia]. Properly targeted, genetic methods may hold promise for avoiding off-target effects such as increased inflammation (Mizumatsu et al., 2003; Monje et al., 2002) or inhibited angiogenesis (Kurzen, Schmitt, Näher, & Möhler, 2003; Monje et al., 2002), which accompany both irradiation and pharmacological knockdown methods. A common thread of behavioral differences in the ability to discriminate between similar events runs throughout recent studies of adult neurogenesis despite these variations in knockdown efficiency and off-target effects.

Taking the above results into consideration, descriptive models for the role of adult neurogenesis in pattern separation generally fall within two, often described as mutually exclusive, frameworks (Aimone, Deng, & Gage, 2010; Becker, 2005; Deng, Aimone, & Gage, 2010; Piatti et al., 2013; Sahay, Wilson, & Hen, 2011; Wiskott, Rasch, & Kempermann, 2006). The first model proposes that immature abDGCs act as individual coding units. As a consequence of low input specificity, immature abDGCs act as pattern integrators, responding to broad input patterns and rate remapping in response to subtle changes in an animal's environment. In turn, through their mossy fiber connections, they directly influence encoding in the CA3 (Aimone et al., 2010). As new neurons mature, they join mature DGCs as sparse coders in the DG and thereby contribute to pattern separation by encoding new representations in a new, orthogonal population of neurons, autonomously maximizing information while minimizing interference (Aimone, Deng, & Gage, 2011; Becker, 2005; Wiskott et al., 2006). The second model proposes a modulatory role whereby new neurons maintain the sparse activity of mature DGCs within the DG. Immature neurons mediate this function through their relative sensitivity to weak inputs. By reactivating for similar environmental stimuli – even if weak – they recruit feedback inhibition targeted toward mature DGCs, presumably via direct or indirect connections to local hilar interneurons (Sahay, Wilson, et al., 2011). This sparsity ensures minimally overlapping memory representations. Increasingly, evidence suggests a paradoxical dual role for adult-born neurons in both processes.

4. New neurons are pattern integrators/broad responders

During maturation, abDGCs go through a critical period of hyperexcitability, enhanced synaptic plasticity, and insensitivity to GABAergic inhibition (Gu et al., 2012; Li, Aimone, Xu, Callaway, & Gage, 2012; Marin-Burgin, Mongiat, Pardi, & Schinder, 2012; Zhao, Deng, & Gage, 2008) while still forming functional connections to CA3 similar to their mature counterparts (Toni et al., 2008; Zhao et al., 2008). During this critical period, immature abDGCs act as pattern integrators as they are activated in response to weak afferent stimulation and continue spiking, whereas mature abDGCs rapidly attenuate their response (Marin-Burgin et al., 2012). Behaviorally, new neurons are more likely to activate to novel stimuli (Kee, Teixeira, Wang, & Frankland, 2007; see Stone et al., 2011 for a dissenting opinion) but, more importantly, abDGCs are proposed to undergo stimulus-specific reactivation for stimuli that the animal experiences while the abDGCs are maturing (Tashiro, Zhao, & Gage, 2007; Trouche, Bontempi, Roullet, & Rampon, 2009). Expanding findings from Deng et al. (2013) to include reactivation of new neurons to enriched environments, results from our lab suggest the same type of preferential reactivation of immature abDGCs and preferential inactivation of mature abDGCs to contexts similar to those in which they matured (Deng et al., unpublished). Mossy fiber synapses further act to filter information coming into the CA3 (Henze et al., 2002; Urban et al., 2001), suggesting that the message hyperactive DGCs convey downstream is likely overrepresented (Alme et al., 2010; Gu et al., 2012; Marin-Burgin et al., 2012). As hyperexcitability declines, abDGCs no longer act as pattern integrators but undergo an abrupt shift and become physiologically indistinguishable from their sparsely activating mature counterparts (Brunner et al., 2014), now contributing to network function by representing the new information states they matured in (Aimone et al., 2011; Becker, 2005; Wiskott et al., 2006). Such new or novel states can be conceptualized in the phase space framework by the addition of discrete valleys to the state space (Fig 3iii).

5. New neurons maintain sparsity

Paradoxically, despite the role of hyperactive immature DGCs as input integrators, manipulations of adult neurogenesis inversely correlate with activity in the DG. Reductions of neurogenesis result in hyperactivity of the DG (Ikrar et al., 2013), and increased neurogenesis results in a suppression of activity in the DG (Ikrar et al., 2013), surprisingly without a change in activity levels downstream in CA3. In vivo, findings further suggest that decreasing neurogenesis increases coordinated activity in the DG (Lacefield, Itskov, Reardon, Hen, & Gordon, 2012), manifested at the cellular level as the recruitment of a larger population of DGCs in response to an environmental stimulus. The selectivity of DGC populations is compromised, leading to greater overlap between populations responsive to distinct contexts and accompanied by an overall increase in firing rate (Rangel et al., 2014). Overall, ablation of adult neurogenesis appears to reduce the inhibitory inputs that heavily suppress activity under normal conditions in the DG (Singer et al., 2011). Taken together with the behavioral studies mentioned above, these results are consistent with the theoretical prediction suggesting that DG sparsity mediates an animal's capacity to discriminate environmental stimuli in pattern separation tasks: hyperactive immature DGCs paradoxically maintain this sparsity and push the DG toward a system of greater pattern separation.

The mechanism by which abDGCs mediate this sparsity remains unclear. However, the balance of excitation to inhibition is likely to play an important role in this process. Immature and mature DGCs functionally innervate GABAergic interneurons that heavily suppress DG activity through feedback inhibition (Acsády, Kamondi, Sík, Freund, & Buzsáki, 1998; Li et al., 2013), whereas immature abDGCs themselves remain partially insensitive to GABA (Li et al., 2012; Zhao et al., 2008). In contrast to mature DGCs, recent work from slice physiology experiments has suggested that immature abDGCs may be limited in their ability to recruit feedback inhibition onto neighboring DGCs (Temprana et al., 2015). The implications of this work in vivo have yet to be clarified. Temprana and colleagues also showed reduced inhibitory drive to immature abDGCs via feedback inhibition from mature DGCs. Determining

whether this reduced feedback inhibition from mature DGCs and hyperexcitability of immature abDGCs counterbalances the immature abDGC's apparently reduced ability to recruit feedback inhibition onto the mature DGC network in vivo will require future experiments. Another recent study has suggested that immature abDGCs transiently form strong connections with inhibitory interneurons in CA3 (Restivo, Niibori, Mercaldo, Josselyn, & Frankland, 2015). Immediate early gene activation in 4-week-old abDGCs was also correlated with that of CA3 interneurons, suggesting that these two populations are coupled in vivo. This study relies heavily on morphological analyses, and physiological validation will be required to resolve this disconnect between slice and in vivo paradigms. The parallel maturation of abDGC-controlled inhibition and abDGC hyperactivity may, therefore, be all the more critical to ensure a balance between excitation and inhibition balance to ensure proper circuit function (Aimone, Wiles, & Gage, 2009; Clemenson et al., 2015; Weisz & Argibay, 2009; Weisz & Argibay, 2012). This balance is most apparent when attempting to interpret the results of Park, Burghardt, Dvorak, Hen, and Fenton (2015). X-ray ablation decreases evoked activity in the DG, suggesting a hyperactive role for abDGCs, but leads to a leftward shift in EPSP-spike coupling upon conflict training (a DG- and adult neurogenesis-dependent task), which the authors use to suggest an inhibitory role for abDGCs that is experience dependent (Park et al., 2015).

6. A dual role for new neurons: Balancing resolution and robustness

In the models above, inhibition mediates sparsity, and sparsity mediates discrimination by avoiding representational overlap. The DG, however, already has mechanisms to limit its activity. Heavy feedback inhibition from mature DGCs and mossy cells, as in much of the rest of the brain, does not have to be dependent on adult neurogenesis. Rather than merely playing a static role in pattern separation, adult neurogenesis may provide the DG with a mechanism to dynamically balance memory resolution and memory robustness by minimizing overlap between memory representations.

In this model, as the richness of an animal's experience increases and memory load becomes more complex, proliferation and survival of abDGCS might be expected to increase in an activity-dependent fashion (Park et al., 2015; Piatti et al., 2011; Stone et al., 2011). This increase in abDGCs results in an overall decrease in DG excitability (Ikrar et al., 2013) and ultimately results in increased sparsity via disynaptic inhibition of the DG network. This increased sparsity increases the number of nonoverlapping representations available to the network, in effect sharpening the state space to allow for increased discrimination and coding of new experiences. The ultimate result of these reallocations is to take smooth portions of the state space, in which it is difficult to discriminate nearby states, and impose roughness to increase memory resolution (Fig 3iii).

Increased sparsity, however, may come at a cost. As memory representations are distributed among fewer neurons, they may become more susceptible to loss through degradation and interference (Weisz & Argibay, 2012). Behaviorally, this process is manifested as forgetting. Recently it has been suggested that adult neurogenesis may mediate a unique form of forgetting (Akers et al., 2014). In this study, increasing neurogenesis after the formation of a memory was shown to inhibit recall of the learned experience, and the authors concluded that forgetting occurred. Adult neurogenesis may, however, permit increased memory resolution without sacrificing memory robustness by adding computational units to the circuit. However, behaviorally differentiating forgetting from increased discrimination may not be straightforward; that is, it is difficult to verify if an animal is *unable* to recall a stimulus or if it is now able to discriminate between two stimuli that the experimenter did not intend to make discriminatable. An animal may no longer see stimuli as equivalent because, as a product of increased pattern separation, it has become more sensitive to minor differences in the environment (Clemenson et al., 2015). Caution should therefore be used in interpreting results of any behavioral assay where forgetting and increased discrimination may lead to the same result. For example, Clemenson et al. used a fear conditioning discrimination paradigm in which the training (shock) context differed from each of two testing contexts. The wire grid floor used to deliver the shock was covered by a plastic insert in both testing contexts. An animal that has forgotten the original conditioning event will not freeze when exposed to the test contexts. However, neither will an animal that notices the floor has changed if it has specifically associated the foot shock with the floor. Similarly, performance during the probe trial of the Morris Water Maze is commonly reported as the percentage of time spent in the quadrant formerly occupied by the platform during training. An animal that spends little time in the target quadrant may have forgotten the original location, or may have been so certain of that location that it explored it once, found the platform to be missing, and continued searching the rest of the maze. To discount this interpretation, some groups report latency to the old platform location as well, but this is not universal. Alternatively, others have viewed these as changes in "cognitive flexibility" (Burghardt, Park, Hen, & Fenton, 2012).

According to the Mixed Coding Hypothesis (Aimone et al., 2011), immature abDGCs initially are low information encoders for broad content, but as they mature they become tightly tuned high information encoders, joining extant DGCs in a sparsely activated distributed code but now encoding novel stimuli, effectively adding new stable valleys to the phase space. The result is to allow the encoding of novel representations while avoiding overlap and interference with the surviving representational network. The task then becomes to differentiate the direct contribution of immature abDGCs, as "pattern integrators" heavily affecting learning and memory downstream, and mature abDGCs, as sparse encoders, from indirect effects on local network activity that then propagate downstream to CA3. These alternative models and behavioral outcomes listed above demonstrate that behavioral assessments of the role of adult neurogenesis are ambiguous when taken alone.

7. Looking forward

Recent work using opto- and chemogenetic manipulations have revolutionized our understanding of the substrates of memory "engrams" (Cowansage et al., 2014; Denny et al., 2014; Garner et al., 2012; Liu et al., 2012; Nabavi et al., 2014; Ramirez et al., 2013; Tonegawa, Liu, Ramirez, & Redondo, 2015). However, these experiments (like IEG experiments before them) have been limited in that they only label a single memory representation for manipulation. The means by which the patterns of activity are segregated and encoded remains unknown [though Nabavi et al. (2014) serves as the greatest evidence supporting a causal role for LTP in memory formation to date, and excitability at the time of encoding appears to influence the recruitment of a neuron into a memory representation; see Han et al., 2007; Han et al., 2009; Sano et al., 2014; Zhou et al., 2009]. The extension of calcium imaging to study memory in hippocampal behavioral tasks (Dombeck, Harvey, Tian, Looger, & Tank, 2010; Rajasethupathy et al., 2015; Ziv et al., 2013) is promising in that it may be the first technique to bridge the gaps between electrophysiological records and IEG experiments, in vivo, as an animal's memory is tested. It provides both the spatial and temporal resolution necessary to rigorously verify computational theories of pattern separation and completion while elucidating

questions about learning and memory as simple as, "What is the minimal unit of a memory?" However, basic questions such as these will not likely yield simple answers. Instead they will undoubtedly uncover complex dynamics as the brain attempts to balance anatomical, physiological, and environmental pressures to produce accurate predictions about, and generate appropriate actions to interact with, the world. A greater question for this system then becomes one of understanding the mechanisms and constraints under which these processes balance encoding and retrieval, discrimination and generalization, and remembering and forgetting. The role of adult neurogenesis, as a critical component of plasticity in the hippocampus when dealing with highly similar stimuli, is likely to yield interesting conclusions about the dynamic regulation of these forces.

Imaging alone, however, is likely insufficient and underscores a greater need for the development of complementary behavioral tasks. Ideal approaches will possess both the capacity to investigate how changes in sparsity contribute to memory resolution and robustness and the ability to target specific populations of abDGCs to further elucidate their direct and indirect contributions to network function. Further development in this area will, in turn, likely require a return to computational theories of pattern separation and completion to generate predictions about the circuit and network level activity that subserves these functions. "Behavior-free" passive imaging paradigms may also prove valuable, as minor network fluctuations may not be behaviorally observable. Future findings could lead to interesting questions such as "Does the animal or the dentate forget first?," as behavioral pattern separation and computational pattern separation, as performed through concerted network activity in the DG and HC, can be directly correlated (for differences between these two types of "pattern separation," see Santoro, 2013). This direction of study may prove all the more interesting as a tractable method to understand more generally how the brain tolerates variation in activity and how coordinated mass action gives rise to behavioral discrimination vis-à-vis pattern separation and completion. These findings will prove computationally relevant in many areas of the brain (Barnes, Hofacer, Zaman, Rennaker, & Wilson, 2008; Bartko, Winters, Cowell, Saksida, & Bussey, 2007a, 2007b; Burke, Wallace, Nematollahi, Uprety, & Barnes, 2010; Gilbert & Kesner, 2002; Gilbert & Kesner, 2003; Marr, 1983; Sahay, Wilson, et al., 2011; Wilson, 2009).

Acknowledgments

We thank Mary Lynn Gage for comments on the manuscript and our funding sources which made this work possible: NIH R01 MH090258, NIH R01 MH095741, JPB Foundation, Annette Merle-Smith, James S. McDonnell Foundation, Mathers Foundation, the Leona M. and Harry B. Helmsley Charitable Trust grant # 2012-PG-MED002, and the Dan and Martina Lewis Biophotonics Fellows Program.

References

Acsády, L., Kamondi, A., Sík, A., Freund, T., & Buzsáki, G. (1998). GABAergic cells are the major postsynaptic targets of mossy fibers in the rat hippocampus. *Journal of Neuroscience, 18*, 3386–3403.

Aimone, J. B., Deng, W., & Gage, F. H. (2010). Adult neurogenesis: Integrating theories and separating functions. *Trends in Cognitive Sciences, 14*, 325–337.

Aimone, J. B., Deng, W., & Gage, F. H. (2011). Resolving new memories: A critical look at the dentate gyrus, adult neurogenesis, and pattern separation. *Neuron, 70*, 589–596.

Aimone, J. B., Wiles, J., & Gage, F. H. (2009). Computational influence of adult neurogenesis on memory encoding. *Neuron, 61*, 187–202.

Akers, K. G., Martinez-Canabal, A., Restivo, L., Yiu, A. P., Cristofaro, A. D., Hsiang, H.-L. (Liz), et al. (2014). Hippocampal neurogenesis regulates forgetting during adulthood and infancy. *Science, 344*, 598–602.

Alme, C. B., Buzzetti, R. A., Marrone, D. F., Leutgeb, J. K., Chawla, M. k., Schaner, M. j., et al. (2010). Hippocampal granule cells opt for early retirement. *Hippocampus, 20*, 1109–1123.

Amaral, D. G., Ishizuka, N., & Claiborne, B. (1990). Neurons, numbers and the hippocampal network. *Progress in Brain Research, 83*, 1–11.

Amit, D. J., Gutfreund, H., & Sompolinsky, H. (1987). Statistical mechanics of neural networks near saturation. *Annalen der Physik, 173*, 30–67.

Barnes, D. C., Hofacer, R. D., Zaman, A. R., Rennaker, R. L., & Wilson, D. A. (2008). Olfactory perceptual stability and discrimination. *Nature Neuroscience, 11*, 1378–1380.

Bartko, S. J., Winters, B. D., Cowell, R. A., Saksida, L. M., & Bussey, T. J. (2007a). Perirhinal cortex resolves feature ambiguity in configural object recognition and perceptual oddity tasks. *Learning & Memory (Cold Spring Harbor, N.Y.), 14*, 821–832.

Bartko, S. J., Winters, B. D., Cowell, R. A., Saksida, L. M., & Bussey, T. J. (2007b). Perceptual functions of perirhinal cortex in rats: Zero-delay object recognition and simultaneous oddity discriminations. *Journal of Neuroscience, 27*, 2548–2559.

Becker, S. (2005). A computational principle for hippocampal learning and neurogenesis. *Hippocampus, 15*, 722–738.

Bergami, M., Masserdotti, G., Temprana, S. G., Motori, E., Eriksson, T. M., Göbel, J., et al. (2015). A critical period for experience-dependent remodeling of adult-born neuron connectivity. *Neuron, 85*, 710–717.

Brunner, J., Neubrandt, M., Van-Weert, S., Andrási, T., Borgmann, F. B. K., Jessberger, S., et al. (2014). Adult-born granule cells mature through two functionally distinct states. *eLife, 3*, e03104.

Burghardt, N. S., Park, E. H., Hen, R., & Fenton, A. A. (2012). Adult-born hippocampal neurons promote cognitive flexibility in mice. *Hippocampus, 22*, 1795–1808.

Burke, S. N., Wallace, J. L., Nematollahi, S., Uprety, A. R., & Barnes, C. A. (2010). Pattern separation deficits may contribute to age-associated recognition impairments. *Behavioral Neuroscience, 124*, 559–573.

Chawla, M. K., Guzowski, J. F., Ramirez-Amaya, V., Lipa, P., Hoffman, K. L., Marriott, L. K., et al. (2005). Sparse, environmentally selective expression of Arc RNA in the upper blade of the rodent fascia dentata by brief spatial experience. *Hippocampus, 15*, 579–586.

Clelland, C. D., Choi, M., Romberg, C., Clemenson, G. D., Fragniere, A., Tyers, P., et al. (2009). A functional role for adult hippocampal neurogenesis in spatial pattern separation. *Science, 325*, 210–213.

Clemenson, G. D., Lee, S. W., Deng, W., Barrera, V. R., Iwamoto, K. S., Fanselow, M. S., et al. (2015). Enrichment rescues contextual discrimination deficit associated with immediate shock. *Hippocampus, 25*, 385–392.

Cowansage, K. K., Shuman, T., Dillingham, B. C., Chang, A., Golshani, P., & Mayford, M. (2014). Direct reactivation of a coherent neocortical memory of context. *Neuron, 84*, 432–441.

Creer, D. J., Romberg, C., Saksida, L. M., van Praag, H., & Bussey, T. J. (2010). Running enhances spatial pattern separation in mice. *Proceedings of the National Academy of Sciences, 107*, 2367–2372.

Deng, W., Aimone, J. B., & Gage, F. H. (2010). New neurons and new memories: How does adult hippocampal neurogenesis affect learning and memory? *Nature Reviews Neuroscience, 11*, 339–350.

Deng, W., Mayford, M., & Gage, F. H. (2013). Selection of distinct populations of dentate granule cells in response to inputs as a mechanism for pattern separation in mice. *eLife, 2*.

Deng, W., Saxe, M. D., Gallina, I. S., & Gage, F. H. (2009). Adult-born hippocampal dentate granule cells undergoing maturation modulate learning and memory in the brain. *Journal of Neuroscience, 29*, 13532–13542.

Denny, C. A., Kheirbek, M. A., Alba, E. L., Tanaka, K. F., Brachman, R. A., Laughman, K. B., et al. (2014). Hippocampal memory traces are differentially modulated by experience, time, and adult neurogenesis. *Neuron, 83*, 189–201.

Deshpande, A., Bergami, M., Ghanem, A., Conzelmann, K.-K., Lepier, A., Götz, M., et al. (2013). Retrograde monosynaptic tracing reveals the temporal evolution of inputs onto new neurons in the adult dentate gyrus and olfactory bulb. *Proceedings of the National Academy of Sciences USA, 110*, E1152–E1161.

Dombeck, D. A., Harvey, C. D., Tian, L., Looger, L. L., & Tank, D. W. (2010). Functional imaging of hippocampal place cells at cellular resolution during virtual navigation. *Nature Neuroscience, 13*, 1433–1440.

Dupret, D., Revest, J.-M., Koehl, M., Ichas, F., De Giorgi, F., Costet, P., et al. (2008). Spatial relational memory requires hippocampal adult neurogenesis. *PLoS ONE, 3*, e1959.

Espósito, M. S., Piatti, V. C., Laplagne, D. A., Morgenstern, N. A., Ferrari, C. C., Pitossi, F. J., et al. (2005). Neuronal differentiation in the adult hippocampus recapitulates embryonic development. *Journal of Neuroscience, 25*, 10074–10086.

Garner, A. R., Rowland, D. C., Hwang, S. Y., Baumgaertel, K., Roth, B. L., Kentros, C., et al. (2012). Generation of a synthetic memory trace. *Science, 335*, 1513–1516.

Garthe, A., Behr, J., & Kempermann, G. (2009). Adult-generated hippocampal neurons allow the flexible use of spatially precise learning strategies. *PLoS ONE, 4*, e5464.

Ge, S., Sailor, K. A., Ming, G., & Song, H. (2008). Synaptic integration and plasticity of new neurons in the adult hippocampus. *Journal of Physiology, 586*, 3759–3765.

Gilbert, P. E., & Kesner, R. P. (2002). The amygdala but not the hippocampus is involved in pattern separation based on reward value. *Neurobiology of Learning and Memory, 77*, 338–353.

Gilbert, P. E., & Kesner, R. P. (2003). Recognition memory for complex visual discriminations is influenced by stimulus interference in rodents with perirhinal cortex damage. *Learning & Memory, 10*, 525–530.

Gilbert, P. E., Kesner, R. P., & Lee, I. (2001). Dissociating hippocampal subregions: Double dissociation between dentate gyrus and CA1. *Hippocampus, 11*, 626–636.

Goodrich-Hunsaker, N. J., Hunsaker, M. R., & Kesner, R. P. (2008). The interactions and dissociations of the dorsal hippocampus subregions: How the dentate gyrus, CA3, and CA1 process spatial information. *Behavioral Neuroscience, 122*, 16–26.

Gothard, K. M., Hoffman, K. L., Battaglia, F. P., & McNaughton, B. L. (2001). Dentate gyrus and ca1 ensemble activity during spatial reference frame shifts in the presence and absence of visual input. *Journal of Neuroscience, 21*, 7284–7292.

Gu, Y., Arruda-Carvalho, M., Wang, J., Janoschka, S. R., Josselyn, S. A., Frankland, P. W., et al. (2012). Optical controlling reveals time-dependent roles for adult-born dentate granule cells. *Nature Neuroscience, 15*, 1700–1706.

Han, J.-H., Kushner, S. A., Yiu, A. P., Cole, C. J., Matynia, A., Brown, R. A., et al. (2007). Neuronal competition and selection during memory formation. *Science, 316*, 457–460.

Han, J.-H., Kushner, S. A., Yiu, A. P., Hsiang, H.-L. (Liz), Buch, T., Waisman, A., et al. (2009). Selective erasure of a fear memory. *Science, 323*, 1492–1496.

Henze, D. A., Wittner, L., & Buzsáki, G. (2002). Single granule cells reliably discharge targets in the hippocampal CA3 network in vivo. *Nature Neuroscience, 5*, 790–795.

Huckleberry, K. A., Kane, G. A., Mathis, R. J., Cook, S. G., Clutton, J. E., & Drew, M. R. (2015). Behavioral experience induces zif268 expression in mature granule cells but suppresses its expression in immature granule cells. *Frontiers in Systems Neuroscience, 9*, 118.

Hunsaker, M. R., Mooy, G. G., Swift, J. S., & Kesner, R. P. (2007). Dissociations of the medial and lateral perforant path projections into dorsal DG, CA3, and CA1 for spatial and nonspatial (visual object) information processing. *Behavioral Neuroscience, 121*, 742–750.

Ikrar, T., Guo, N., He, K., Besnard, A., Levinson, S., Hill, A., et al. (2013). Adult neurogenesis modifies excitability of the dentate gyrus. *Frontiers in Neural Circuits, 7*, 204.

Jessberger, S., Clark, R. E., Broadbent, N. J., Clemenson, G. D., Consiglio, A., Lie, D. C., et al. (2009). Dentate gyrus-specific knockdown of adult neurogenesis impairs spatial and object recognition memory in adult rats. *Learning & Memory (Cold Spring Harbor, N.Y.), 16*, 147–154.

Jessberger, S., & Kempermann, G. (2003). Adult-born hippocampal neurons mature into activity-dependent responsiveness. *European Journal of Neuroscience, 18*, 2707–2712.

Jung, M. W., & McNaughton, B. L. (1993). Spatial selectivity of unit activity in the hippocampal granular layer. *Hippocampus, 3*, 165–182.

Kee, N., Teixeira, C. M., Wang, A. H., & Frankland, P. W. (2007). Preferential incorporation of adult-generated granule cells into spatial memory networks in the dentate gyrus. *Nature Neuroscience, 10*, 355–362.

Kesner, R. P. (2007). A behavioral analysis of dentate gyrus function. In H. E. Scharfman (Ed.), *Progress in brain research* (pp. 567–576). Elsevier.

Kurzen, H., Schmitt, S., Näher, H., & Möhler, T. (2003). Inhibition of angiogenesis by non-toxic doses of temozolomide. *Anti-Cancer Drugs, 14*, 515–522.

Lacefield, C. O., Itskov, V., Reardon, T., Hen, R., & Gordon, J. A. (2012). Effects of adult-generated granule cells on coordinated network activity in the dentate gyrus. *Hippocampus, 22*, 106–116.

Lassalle, J. M., Bataille, T., & Halley, H. (2000). Reversible inactivation of the hippocampal mossy fiber synapses in mice impairs spatial learning, but neither consolidation nor memory retrieval, in the Morris navigation task. *Neurobiology of Learning and Memory, 73*, 243–257.

Lee, I., & Kesner, R. P. (2004). Encoding versus retrieval of spatial memory: Double dissociation between the dentate gyrus and the perforant path inputs into CA3 in the dorsal hippocampus. *Hippocampus, 14*, 66–76.

Leutgeb, S., Leutgeb, J. K., Barnes, C. A., Moser, E. I., McNaughton, B. L., & Moser, M.-B. (2005). Independent codes for spatial and episodic memory in hippocampal neuronal ensembles. *Science, 309*, 619–623.

Leutgeb, J. K., Leutgeb, S., Moser, M.-B., & Moser, E. I. (2007). Pattern separation in the dentate gyrus and CA3 of the hippocampus. *Science, 315*, 961–966.

Leutgeb, J. K., Leutgeb, S., Treves, A., Meyer, R., Barnes, C. A., McNaughton, B. L., et al. (2005). Progressive transformation of hippocampal neuronal representations in "Morphed" environments. *Neuron, 48*, 345–358.

Li, Y., Aimone, J. B., Xu, X., Callaway, E. M., & Gage, F. H. (2012). Development of GABAergic inputs controls the contribution of maturing neurons to the adult hippocampal network. *Proceedings of the National Academy of Sciences, 109*, 4290–4295.

Li, Y., Stam, F. J., Aimone, J. B., Goulding, M., Callaway, E. M., & Gage, F. H. (2013). Molecular layer perforant path-associated cells contribute to feed-forward inhibition in the adult dentate gyrus. *Proceedings of the National Academy of Sciences USA, 110*, 9106–9111.

Lisman, J. E. (1999). Relating hippocampal circuitry to function: Recall of memory sequences by reciprocal dentate–CA3 interactions. *Neuron, 22*, 233–242.

Liu, X., Ramirez, S., Pang, P. T., Puryear, C. B., Govindarajan, A., Deisseroth, K., et al. (2012). Optogenetic stimulation of a hippocampal engram activates fear memory recall. *Nature, 484*, 381–385.

Marin-Burgin, A., Mongiat, L. A., Pardi, M. B., & Schinder, A. F. (2012). Unique processing during a period of high excitation/inhibition balance in adult-born neurons. *Science, 335*, 1238–1242.

Marr, D. (1971). Simple memory: A theory for archicortex. *Philosophical Transactions of the Royal Society B: Biological Sciences, 262*, 23–81.

Marr, D. (1983). *Vision: A computational investigation into the human representation and processing of visual information*. Henry Holt and Company.

McClelland, J. L., McNaughton, B. L., & O'Reilly, R. C. (1995). Why there are complementary learning systems in the hippocampus and neocortex: Insights from the successes and failures of connectionist models of learning and memory. *Psychological Review, 102*, 419–457.

McCloskey, M., & Cohen, N. (1989). Catastrophic interference in connectionist networks: The sequential learning problem. *Psychology of Learning and Motivation, 24*, 109–164.

McHugh, T. J., Jones, M. W., Quinn, J. J., Balthasar, N., Coppari, R., Elmquist, J. K., et al. (2007). Dentate gyrus NMDA receptors mediate rapid pattern separation in the hippocampal network. *Science, 317*, 94–99.

Ming, G.-L., & Song, H. (2011). Adult neurogenesis in the mammalian brain: Significant answers and significant questions. *Neuron, 70*, 687–702.

Mizumatsu, S., Monje, M. L., Morhardt, D. R., Rola, R., Palmer, T. D., & Fike, J. R. (2003). Extreme sensitivity of adult neurogenesis to low doses of X-irradiation. *Cancer Research, 63*, 4021–4027.

Monje, M. L., Mizumatsu, S., Fike, J. R., & Palmer, T. D. (2002). Irradiation induces neural precursor-cell dysfunction. *Nature Medicine, 8*, 955–962.

Mulders, W. H., West, M. J., & Slomianka, L. (1997). Neuron numbers in the presubiculum, parasubiculum, and entorhinal area of the rat. *Journal of Comparative Neurology, 385*, 83–94.

Nabavi, S., Fox, R., Proulx, C. D., Lin, J. Y., Tsien, R. Y., & Malinow, R. (2014). *Engineering a memory with LTD and LTP*. Nature Advance Online Publication.

Nakashiba, T., Cushman, J. D., Pelkey, K. A., Renaudineau, S., Buhl, D. L., McHugh, T. J., et al. (2012). Young dentate granule cells mediate pattern separation, whereas old granule cells facilitate pattern completion. *Cell, 149*, 188–201.

Neunuebel, J. P., & Knierim, J. J. (2012). Spatial firing correlates of physiologically distinct cell types of the rat dentate gyrus. *Journal of Neuroscience, 32*, 3848–3858.

O'Reilly, R. C., & McClelland, J. L. (1994). Hippocampal conjunctive encoding, storage, and recall: Avoiding a trade-off. *Hippocampus, 4*, 661–682.

Park, E. H., Burghardt, N. S., Dvorak, D., Hen, R., & Fenton, A. A. (2015). Experience-dependent regulation of dentate gyrus excitability by adult-born granule cells. *Journal of Neuroscience, 35*, 11656–11666.

Piatti, V. C., Davies-Sala, M. G., Espósito, M. S., Mongiat, L. A., Trinchero, M. F., & Schinder, A. F. (2011). The timing for neuronal maturation in the adult hippocampus is modulated by local network activity. *Journal of Neuroscience, 31*, 7715–7728.

Piatti, V. C., Ewell, L. A., & Leutgeb, J. K. (2013). Neurogenesis in the dentate gyrus: Carrying the message or dictating the tone. *Frontiers in Neuroscience, 7*.

Poucet, B., & Save, E. (2005). Attractors in memory. *Science, 308*, 799–800.

Rajasethupathy, P., Sankaran, S., Marshel, J. H., Kim, C. K., Ferenczi, E., Lee, S. Y., et al. (2015). Projections from neocortex mediate top-down control of memory retrieval. *Nature, 526*, 653–659.

Ramirez, S., Liu, X., Lin, P.-A., Suh, J., Pignatelli, M., Redondo, R. L., et al. (2013). Creating a false memory in the hippocampus. *Science, 341*, 387–391.

Rangel, L. M., Alexander, A. S., Aimone, J. B., Wiles, J., Gage, F. H., Chiba, A. A., et al. (2014). Temporally selective contextual encoding in the dentate gyrus of the hippocampus. *Nature Communications, 5*.

Rennó-Costa, C., Lisman, J. E., & Verschure, P. F. M. J. (2010). The mechanism of rate remapping in the dentate gyrus. *Neuron, 68*, 1051–1058.

Restivo, L., Niibori, Y., Mercaldo, V., Josselyn, S. A., & Frankland, P. W. (2015). Development of adult-generated cell connectivity with excitatory and inhibitory cell populations in the hippocampus. *Journal of Neuroscience, 35*, 10600–10612.

Rolls, E. T., & Kesner, R. P. (2006). A computational theory of hippocampal function, and empirical tests of the theory. *Progress in Neurobiology, 79*, 1–48.

Sahay, A., Scobie, K. N., Hill, A. S., O'Carroll, C. M., Kheirbek, M. A., Burghardt, N. S., et al. (2011). Increasing adult hippocampal neurogenesis is sufficient to improve pattern separation. *Nature, 472*, 466–470.

Sahay, A., Wilson, D. A., & Hen, R. (2011). Pattern separation: A common function for new neurons in hippocampus and olfactory bulb. *Neuron, 70*, 582–588.

Sano, Y., Shobe, J. L., Zhou, M., Huang, S., Shuman, T., Cai, D. J., et al. (2014). CREB regulates memory allocation in the insular cortex. *Current Biology, 24*, 2833–2837.

Santoro, A. (2013). Reassessing pattern separation in the dentate gyrus. *Frontiers in Behavioral Neuroscience, 7*.

Saxe, M. D., Malleret, G., Vronskaya, S., Mendez, I., Garcia, A. D., Sofroniew, M. V., et al. (2007). Paradoxical influence of hippocampal neurogenesis on working memory. *Proceedings of the National Academy of Sciences USA, 104*, 4642–4646.

Schmidt, B., Marrone, D. F., & Markus, E. J. (2012). Disambiguating the similar: The dentate gyrus and pattern separation. *Behavioural Brain Research, 226*, 56–65.

Schmidt-Hieber, C., Jonas, P., & Bischofberger, J. (2004). Enhanced synaptic plasticity in newly generated granule cells of the adult hippocampus. *Nature, 429*, 184–187.

Schoenenberger, P., Gerosa, D., & Oertner, T. G. (2009). Temporal control of immediate early gene induction by light. *PLoS ONE, 4*, e8185.

Shors, T. J., Miesegaes, G., Beylin, A., Zhao, M., Rydel, T., & Gould, E. (2001). Neurogenesis in the adult is involved in the formation of trace memories. *Nature, 410*, 372–376.

Singer, B. H., Gamelli, A. E., Fuller, C. L., Temme, S. J., Parent, J. M., & Murphy, G. G. (2011). Compensatory network changes in the dentate gyrus restore long-term potentiation following ablation of neurogenesis in young-adult mice. *Proceedings of the National Academy of Sciences USA, 108*, 5437–5442.

Snyder, J. S., Choe, J. S., Clifford, M. A., Jeurling, S. I., Hurley, P., Brown, A., et al. (2009). Adult-born hippocampal neurons are more numerous, faster maturing, and more involved in behavior in rats than in mice. *Journal of Neuroscience, 29*, 14484–14495.

Snyder, J. S., Glover, L. R., Sanzone, K. M., Kamhi, J. F., & Cameron, H. A. (2009). The effects of exercise and stress on the survival and maturation of adult-generated granule cells. *Hippocampus, 19*, 898–906.
Stone, S. S. D., Teixeira, C. M., Devito, L. M., Zaslavsky, K., Josselyn, S. A., Lozano, A. M., et al. (2011). Stimulation of entorhinal cortex promotes adult neurogenesis and facilitates spatial memory. *Journal of Neuroscience, 31*, 13469–13484.
Tashiro, A., Zhao, C., & Gage, F. H. (2007). Retrovirus-mediated single-cell gene knockout technique in adult newborn neurons in vivo. *Nature Protocols, 1*, 3049–3055.
Temprana, S. G., Mongiat, L. A., Yang, S. M., Trinchero, M. F., Alvarez, D. D., Kropff, E., ... Schinder, A. F. (2015). Delayed coupling to feedback inhibition during a critical period for the integration of adult-born granule cells. *Neuron, 85*, 116–130.
Tonegawa, S., Liu, X., Ramirez, S., & Redondo, R. (2015). Memory engram cells have come of age. *Neuron, 87*, 918–931.
Toni, N., Laplagne, D. A., Zhao, C., Lombardi, G., Ribak, C. E., Gage, F. H., et al. (2008). Neurons born in the adult dentate gyrus form functional synapses with target cells. *Nature Neuroscience, 11*, 901–907.
Treves, A., & Rolls, E. T. (1994). Computational analysis of the role of the hippocampus in memory. *Hippocampus, 4*, 374–391.
Tronel, S., Belnoue, L., Grosjean, N., Revest, J.-M., Piazza, P.-V., Koehl, M., et al. (2012). Adult-born neurons are necessary for extended contextual discrimination. *Hippocampus, 22*, 292–298.
Trouche, S., Bontempi, B., Roullet, P., & Rampon, C. (2009). Recruitment of adult-generated neurons into functional hippocampal networks contributes to updating and strengthening of spatial memory. *Proceedings of the National Academy of Sciences*. http://dx.doi.org/10.1073/pnas.0811054106.
Urban, N. N., Henze, D. A., & Barrionuevo, G. (2001). Revisiting the role of the hippocampal mossy fiber synapse. *Hippocampus, 11*, 408–417.
Weisz, V. I., & Argibay, P. F. (2009). A putative role for neurogenesis in neuro-computational terms: Inferences from a hippocampal model. *Cognition, 112*, 229–240.
Weisz, V. I., & Argibay, P. F. (2012). Neurogenesis interferes with the retrieval of remote memories: Forgetting in neurocomputational terms. *Cognition, 125*, 13–25.
Wills, T. J., Lever, C., Cacucci, F., Burgess, N., & O'Keefe, J. (2005). Attractor dynamics in the hippocampal representation of the local environment. *Science, 308*, 873–876.
Wilson, D. A. (2009). Pattern separation and completion in olfaction. *Annals of the New York Academy of Sciences, 1170*, 306–312.
Wiskott, L., Rasch, M. J., & Kempermann, G. (2006). A functional hypothesis for adult hippocampal neurogenesis: Avoidance of catastrophic interference in the dentate gyrus. *Hippocampus, 16*, 329–343.
Wojtowicz, J. M., Askew, M. L., & Winocur, G. (2008). The effects of running and of inhibiting adult neurogenesis on learning and memory in rats. *European Journal of Neuroscience, 27*, 1494–1502.
Yassa, M. A., & Stark, C. E. L. (2011). Pattern separation in the hippocampus. *Trends in Neurosciences, 34*, 515–525.
Zhao, C., Deng, W., & Gage, F. H. (2008). Mechanisms and functional implications of adult neurogenesis. *Cell, 132*, 645–660.
Zhou, Y., Won, J., Karlsson, M. G., Zhou, M., Rogerson, T., Balaji, J., et al. (2009). CREB regulates excitability and the allocation of memory to subsets of neurons in the amygdala. *Nature Neuroscience, 12*, 1438–1443.
Ziv, Y., Burns, L. D., Cocker, E. D., Hamel, E. O., Ghosh, K. K., Kitch, L. J., et al. (2013). Long-term dynamics of CA1 hippocampal place codes. *Nature Neuroscience, 16*, 264–266.

Glossary

Adult neurogenesis: the process by which new neurons are continually generated from neural stem cells throughout adulthood. Known to occur in the subventricular zone (giving rise to olfactory bulb neurons) and in the subgranular zone (giving rise to dentate granule cells)

Attractor network: a recurrently connected network whose dynamics give rise to stable patterns (attractor states). Different initial states will settle into a final state that is a local energy minimum (for greater detail see Information Box "Attractor Networks of Memory")

Interference: the disruption or complete elimination of prior learning resulting from new learning. In networks, this results from the rapid adjustment of connections used for encoding the prior learning to accommodate the new learning

Pattern separation: the process by which distinct, but often overlapping or highly similar patterns of neuronal inputs are transformed into distinct neuronal representations

Pattern completion: the process by which a full memory representation is evoked from a partial set of inputs. A corollary of this idea is that similar neuronal inputs will result in the same neural representation

Resolution: the extent of information (or details) encoded by a network of neurons. Increased resolution increases the capability of the system to distinguish, find, or encode details

Robustness: the resistance of a memory representation to being lost, often through degradation and interference

Chapter 1, in full, is a reprint of the material as it appears in: Johnston ST, Shtrahman M, Parylak S, Gonçalves JT, Gage FH. (2016) Paradox of pattern separation and adult neurogenesis: A dual role for new neurons balancing memory resolution and robustness. *Neurobiology of Learning and Memory,* 129 60-68, https://doi.org/10.1016/j.nlm.2015.10.013 . The dissertation author was the primary investigator and author of this paper.

CHAPTER 2: AAV-Induced Toxicity in Neural Progenitor Cells within the Adult Murine Hippocampus

ABSTRACT

Recombinant AAV (rAAV) has been proposed as a safe genetic tool for use in human gene therapy and has seen wide use as a viral vector across nearly all fields of experimental mammalian biology. We demonstrate that neural progenitor cells (NPCs) and immature dentate granule cells (DGCs) within the adult murine hippocampus are particularly sensitive to rAAV-induced cell-death. Cell loss is dose-dependent and nearly complete at experimentally relevant viral titers. rAAV-induced cell-death is rapid and persistent, with loss of BrdU labeled cells within 18 hours post-injection and no evidence of recovery of adult neurogenesis when assessed at 3 months post-injection. The remaining mature DGCs appear hyperactive 4 weeks post-injection based on immediate early gene expression, consistent with previous studies investigating the effects of attenuating adult neurogenesis. *In vitro* application of AAV or electroporation of AAV2 inverted terminal repeats (ITRs) is sufficient to induce cell death. Efficient transduction of the dentate gyrus (DG)—without ablating adult neurogenesis—can be achieved by injection of rAAV2-retro serotyped virus into CA3. rAAV2-retro results in efficient retrograde labeling of mature DGCs and permits *in vivo* 2-photon calcium imaging of dentate activity while leaving adult neurogenesis intact. These findings expand on recent reports implicating rAAV linked toxicity in stem cells and other cell types and suggests future work using rAAV in the DG should be carefully evaluated.

Johnston ST[1, 2], Parylak SL[2], Kim S[2], Mac N[2], Lim CK[2], Gallina IS[2], Bloyd CW[2], Newberry A[2], Saavedra CD[2], Novák O[3], Gonçalves JT[4], Gage FH[1, 2], Shtrahman M[2,5]

[1]Neurosciences Graduate Program, University of California – La Jolla, CA, USA

[2]Laboratory of Genetics, Salk Institute for Biological Studies, La Jolla, CA, USA

[3]Laboratory of Experimental Epileptology, Department of Physiology, Second Faculty of Medicine, Charles University – Prague, CZ

[4]Department of Neuroscience, Albert Einstein College of Medicine, Bronx, NY USA

[5]Department of Neurosciences, University of California - La Jolla, CA USA

INTRODUCTION

The subgranular zone (SGZ) of the hippocampal dentate gyrus (DG) is one of only a few regions of the mammalian brain which continues to exhibit neurogenesis into adulthood. These adult-born neurons (abDGCs) are a heterogeneous population of cells continuously generated from a pool of neural stem cells that progress from quiescence to proliferation, fate specification, and differentiation before maturing into neurons which are indistinguishable from the population of developmentally derived, mature dentate granule cells (DGCs) extant within the DG (Gonçalves et al., 2016a; Kempermann et al., 2015). These cells are sensitive to environmental stimuli with proliferation, survival, dendritic outgrowth and synapse formation regulated *in vivo* by experience, stress, and inflammation (Gonçalves et al., 2016b; Kempermann et al., 2015; Monje et al., 2003; Snyder et al., 2009; Vivar et al.). Numerous studies have demonstrated the contribution of abDGCs to hippocampus-dependent behaviors (Akers et al., 2014; Clelland et al., 2009; Clemenson et al., 2015; Deng et al., 2009, 2010, Ikrar et al., 2013, 2013; Ko et al., 2009; Lacefield et al., 2012; Nakashiba et al., 2012; Sahay et al., 2011; Saxe et al., 2007; Singer et al., 2011; Tronel et al., 2012).

Experimentally identifying abDGCs *in vivo* has proven difficult due to their rarity, the limited time window of maturation, and the lack of a single, universally-accepted marker protein

to distinguish the population. Many studies have thus relied upon post-mortem or *ex vivo* tissues. In a few studies, *in vivo* optical methods have recently permitted the proliferation and development of abDGCs to be structurally resolved (Gonçalves et al., 2016b; Pilz et al., 2018) and dentate and hilar activity to be quantified (Anacker et al., 2018; Danielson et al., 2016, 2017; Hayashi et al., 2017; Kirschen et al., 2017; Pilz et al., 2016). These functional studies represented a step forward to disambiguate an otherwise heterogeneous population of cells (Danielson et al., 2017; GoodSmith et al., 2017; Leutgeb et al., 2007; Nakazawa, 2017; Senzai and Buzsáki, 2017).

A key tool enabling recent *in vivo* optical imaging studies is recombinant adeno-associated virus (rAAV). Adeno-associated virus is an endemic human and primate virus previously proposed to have no known pathogenicity, despite increasing and widespread use (Büning and Schmidt, 2015; Choudhury et al., 2017; Hocquemiller et al., 2016; Hudry and Vandenberghe, 2019). Recombinant AAV allows delivery of target genes, including calcium sensors for *in vivo* imaging, to specific brain regions. However, rAAV has increasingly been reported to have its own intrinsic toxicity in some tissue types (Hinderer et al., 2018; Hirsch et al., 2011; Hordeaux et al., 2018). The toxic effects of rAAV on this circuit have not been assessed (Danielson et al., 2016; Hayashi et al., 2017; Liu et al., 2012; Pilz et al., 2016; Ramirez et al., 2013; Swiech et al., 2015; Zhu et al., 2014). Motivated by our own efforts to study the role of adult neurogenesis in DG function and hippocampus-dependent behavior, we discovered that neural progenitor cells (NPCs) in the DG are highly sensitive to rAAV-induced death at experimentally relevant titers. We further introduce a method using the rAAV2-retro serotype (Tervo et al., 2016) which permits *in vivo* 2-photon calcium imaging of mature DGCs while leaving adult neurogenesis intact.

RESULTS

rAAV attenuates hippocampal adult-neurogenesis

Driven by our own attempts to perform 2-photon calcium imaging on DGCs and our interest in the modulation of DG activity by adult-born DGCs (abDGCs) we found that the delivery of calcium indicators using AAV at doses equivalent to or below previously reported doses resulted in ablation of adult neurogenesis (**Fig. S2.1A**). This effect was robust regardless of vector production facility (Salk Viral Vector Core, U Penn Vector Core, Addgene), purification method (iodixanol, CsCl), capsid serotype (AAV1 & AAV8-shown; AAV9-not shown), promoter (CAG, Syn, CamkIIa), and protein expression (GFP (**Fig. 2.1**), jRGECO, mCherry – shown; Gcamp3, Gcamp6 (variants), tdTomato– not shown) at doses typically required for the functional manipulation or visualization of DGCs *in vivo*.

To systematically quantify the effect of rAAV transduction on abDGCs, we chose to inject a widely available, minimally-expressing cre-recombinase dependent virus (AAV1-CAG-flex-eGFP, U. Penn. & Addgene) in non-cre-expressing C57BL/6 mice to mitigate contributions from toxicity that might be attributed to protein expression. Mice received daily injections of 5-bromo-2'-deoxyuridine (BrdU) for 3 days to label abDGCs, then 1µL of 3E12 GC/mL rAAV was injected unilaterally into the DG immediately (0d), one week, or two weeks later (schematic in **Fig. 2.1A**). Cells three days old and younger are almost completely eliminated within 48 hours (-83.9% ± 6.7%, $p < 0.0001$). Cells that are 8 to 10 days old are partially protected (-41.3% ± 6.3%, $p < 0.0001$), while cells that are 15 to 17 days old are largely protected with variable but non-significant loss (15.4% ± 6.3%, $p = 0.0731$; **Fig. 2.1B**).

We then assessed the effect of titer on rAAV-induced cell loss by labeling abDGCs for three days with BrdU and injecting 1µL 3E12 GC/mL, 1 E12 GC/mL, or 3 E11 GC/mL rAAV

Fig. 2.1. rAAV attenuates hippocampal adult-neurogenesis A) Experimental design of rAAV injection into DG immediately following labeling of adult-born DGCs with BrdU. **B)** Cells birth-dated with BrdU 3 days immediately preceding viral injection show near complete elimination following rAAV injection, cells born 1 week before viral injection are reduced ~50%, and cells born 2 weeks before rAAV injection are modestly diminished. **C)** Experimental design of dose-dependent attenuation of abDGCs by rAAV. **D)** Immediately following birth-dating of BrdU+ abDGCs, a near complete ablation of BrdU+ cells is seen in DG injected with 1μL 3E12 GC/mL rAAV, partial ablation of BrdU+ cells results from the injection of 1μL 1E12 GC/mL rAAV, and a small but significant reduction of adult neurogenesis results from injection of 1μL 3E11 GC/mL rAAV. This pattern is matched by DCX expression (Fig. S2.1B). **E)** Mature DGCs are hyperactive following rAAV-induced cell loss in a dose-dependent manner for injected titers between 3E12 and 3E11 4 weeks after rAAV injection. abDGC knockdown efficiency is significantly correlated with cFOS activation in mature DGCs (Fig. S2.1C). Data are represented as mean ± s.e.m.

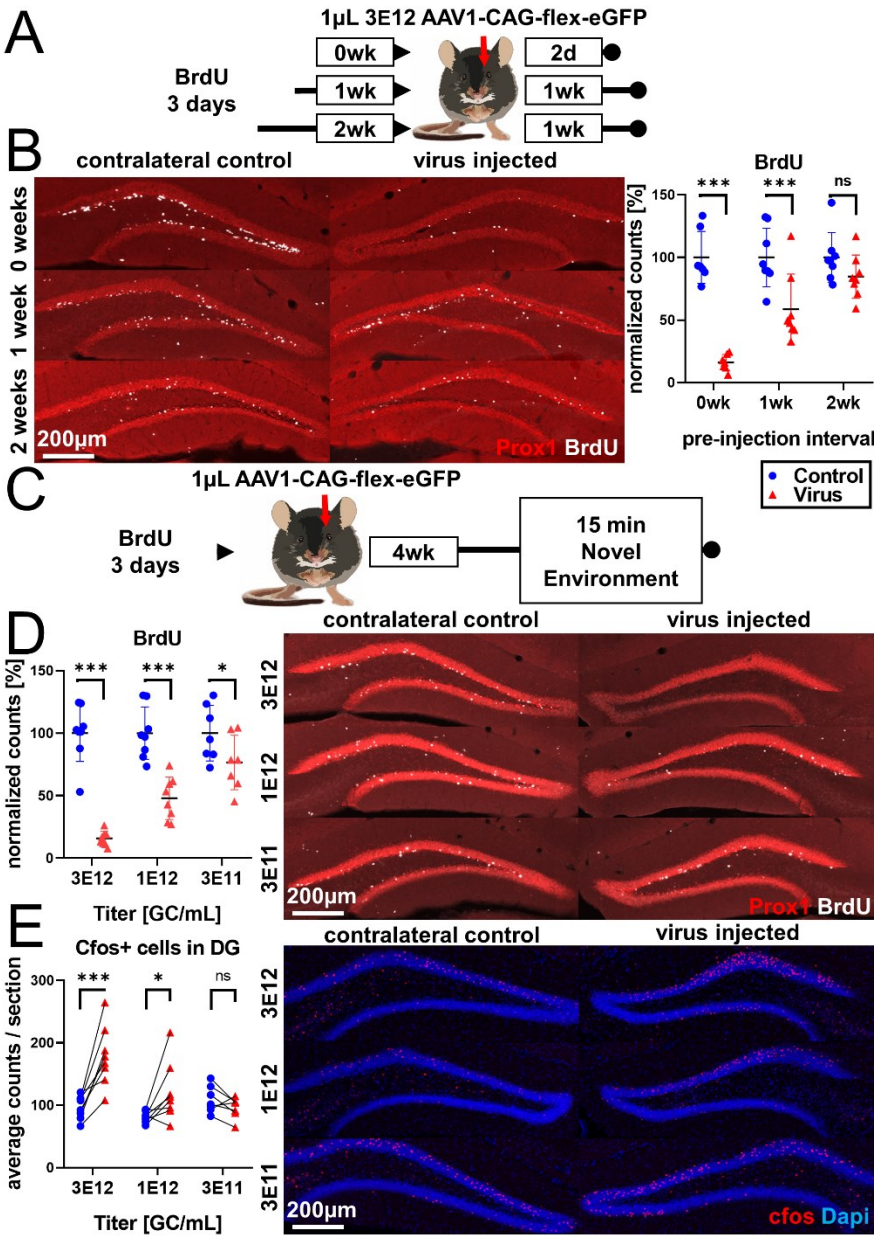
A
1µL 3E12 AAV1-CAG-flex-eGFP
BrdU
3 days
0wk
1wk
2wk
2d
1wk
1wk
B
contralateral control
virus injected
2 weeks 1 week 0 weeks
200µm
Prox1 BrdU
BrdU
normalized counts [%]
***
***
ns
0wk
1wk
2wk
pre-injection interval
Control
Virus
C
1µL AAV1-CAG-flex-eGFP
BrdU
3 days
4wk
15 min
Novel
Environment
D
BrdU
normalized counts [%]
***
***
*
3E12
1E12
3E11
Titer [GC/mL]
contralateral control
virus injected
3E12
1E12
3E11
200µm
Prox1 BrdU
E
Cfos+ cells in DG
average counts / section
***
*
ns
3E12
1E12
3E11
Titer [GC/mL]
contralateral control
virus injected
3E12
1E12
3E11
200µm
cfos Dapi

diluted in sterile saline on the final day (schematic in **Fig. 2.1C**). A nearly complete ablation of BrdU+ cells is seen in the DG injected with 1uL 3E12 GC/mL rAAV (-84.3% ± 6.7%, p <0.0001), while partial ablation of BrdU+ cells results from the injection of 1µL 1E12 GC/mL rAAV (-52.1% ± 6.7%, p <0.0001), and a small but significant reduction of adult neurogenesis results from injection of 1µL 3E11 GC/mL rAAV (-23.4% ± 7.2%, p= 0.012). This pattern is matched by reductions of immature neuron marker DCX expression (**Fig. S2.1B**). To determine if the loss of ~4 week old abDGCs had functional consequences for DG activity, animals were given a Novel Environment (NE) exposure prior to sacrifice, and expression of the immediate early gene (IEG) cFOS was assessed. Consistent with previous studies examining the effects of manipulating adult neurogenesis on DG activity, mature DGC cFOS activation showed an inverse relationship with the level of attenuation of adult neurogenesis. DG injected with 1µL 3E12 GC/mL rAAV resulted in increased mature DGC cFOS activation (+81.6±13.6 cells per section, p <0.0001), 1µL 1E12 GC/mL rAAV resulted in a moderate and more variable increase (+40.0 ± 13.6 cells per section, p=0.24), and 1µL 3E11 GC/mL rAAV demonstrated no measurable effect (+13.3 ± 14.5 cells per section, n.s.). cFOS activation and loss of BrdU+ cells are significantly correlated (slope =0.26, R2=0.59, p<0.0001; **Fig. S2.1C**).

Impact of neurogenesis stage on susceptibility to rAAV-induced cell loss.

To determine the population of cells susceptible to rAAV-induced loss we undertook a series of experiments altering post-injection interval and measuring canonical early, middle, and late histological markers associated with NPC development in the DG. Following labeling with BrdU, mice were unilaterally injected with 1µL 3E12 GC/mL rAAV and sacrificed at 2 days, 1 week, or 4 weeks post-injection (schematic in **Fig. 2.2A**). Sox2+ cells within the SGZ and hilus

were modestly decreased (treatment -14.4% ± 3.7%, p<0.0001; interaction n.s.) at 2 days (-18.9% ± 6.5%, p= 0.026) and 1 week (-21.9% ± 6.1%, p= 0.006) following rAAV injection, but not at 4 weeks post-injection (-2.5% ± 6.5%, n.s.; **Fig. 2.2B,C**). Tbr2+ intermediate progenitor cells are almost entirely lost (treatment -75.5% ± 6.6%, p<0.001; interaction n.s.) within 2 days of rAAV injection and do not recover by 4 weeks post-injection (2 days: -80.2% ± 11.8% , p<0.0001; 1 week: 76.9% ± 11%, p<0.0001; 4 weeks: -69.4% ± 11.8%, p<0.0001; **Fig. 2.2B, D**). Intensity of the late premitotic and immature neuronal marker DCX shows progressive decline until complete loss at 4 weeks post-injection (treatment: 59.5% ± 4.5%, p<0.0001; interaction: p<0.0001; 2 days: -27.7% ± 8.0%, p=0.0077; 1 week: 58.7% ± 7.5%, p<0.0001; 4 weeks: -92.0% ± 8.0%, p<0.0001; **Fig. 2.2B, E**), and does not recover by 3 months post-injection (**Fig. S2.1D**). Taken together this suggests initial sensitivity of some Sox2+ cells to rAAV transduction, but the progenitor pool remains largely intact. Instead, a rapid loss of Tbr2+ intermediate progenitors by 2 days largely drives rAAV-induced toxicity. The decline of the DCX+ immature neuron population over time suggests that loss of the Tbr2+ progenitor pool prevents neurogenesis from progressing beyond intermediate progenitors to the neuroblast stage (mirroring the loss seen in **Fig. 2.1A, S1B**).

Given the extensive and rapid loss of BrdU+ (**Fig. 2.1B**) and Tbr2+ (**Fig. 2.2B,D**) cells, we designed an acute time-course experiment to determine the mechanism of rAAV-induced cell loss (schematic **Fig. 2.2G**). Following labeling with BrdU animals were injected bilaterally, with 1µL 3E12 rAAV into one dorsal DG and 1µL saline into the contralateral DG to control for the acute effect of surgery-induced inflammation and cell-loss. rAAV-injected DGs had fewer BrdU+ cells at 12 and 18 hours relative to their contralateral saline control treatment: -27.9% ±

Fig. 2.2 Impact of neurogenesis stage on susceptibility to rAAV-induced cell loss (A) Experimental design to assess the effect of rAAV post-injection interval on cell-loss – following labeling with BrdU, mice are injected unilaterally with 1µL 3E12 GC/mL rAAV and sacrificed at 2 days, 1 week, or 4 weeks. **(B)** Representative histological staining of neural progenitor and immature neuronal markers Sox2 (white, upper panels), DCX (red, upper panels), and Tbr2 (white, lower panels) following rAAV injection. **(C)** Sox2+ neural stem cells within the SGZ are slightly reduced 2 days and 1 week following rAAV injection, but not at 4 weeks post-injection. **(D)** Tbr2+ intermediate progenitor cells are lost within 2 days of rAAV injection and do not recover by 4 weeks post-injection. **(E)** Immature neuronal marker DCX intensity shows progressive decline until complete loss at 4 weeks post-injection. **(F)** Injection of 1µL of an equivalent number of empty AAV capsids does not result in loss of Tbr2+ intermediate progenitors 2 weeks post-injection. **(G)** Experimental design for acute timeline of rAAV-induced cell loss – following labeling with BrdU, 1µL 3E12 GC/mL rAAV or saline control are injected into contralateral sides of DG, mice are sacrificed at 12 and 18 hours, Tbr2 immunoreactivity and DNA condensation and nuclear fragmentation (pyknosis and karyorrhexis, white arrow) is assessed with BrdU (green) & Caspase 3 activation (red). 10µm scale bar (white, lower right). **(H)** BrdU+ cells show variable decline 12 hours after rAAV injection and significant decline at 18 hours relative to saline control. **(I)** Tbr2+ intermediate progenitors show significant decline by 18 hours following rAAV injection. **(J)** BrdU+ cells exhibit a significant increase in pyknosis 12 hours after rAAV injection. An increase in pyknotic and Caspase 3+ pyknotic cells is seen at 12 hours (Fig. S2.2F-H). Data are represented as mean ± s.e.m.

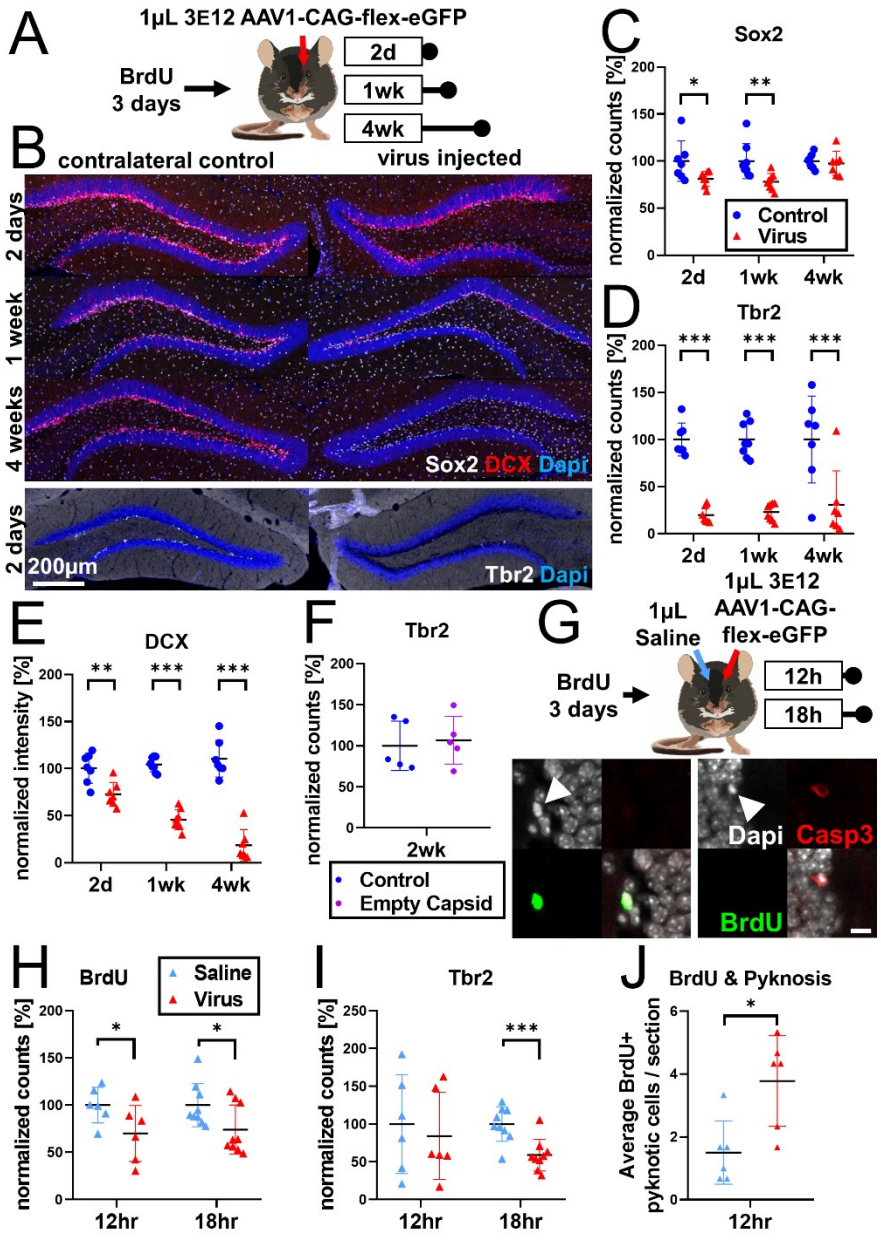
A
1µL 3E12 AAV1-CAG-flex-eGFP
BrdU
3 days
2d
1wk
4wk
B
contralateral control
virus injected
2 days
1 week
4 weeks
Sox2 DCX Dapi
2 days
200µm
Tbr2 Dapi
C
Sox2
normalized counts [%]
Control
Virus
2d
1wk
4wk
D
Tbr2
normalized counts [%]
2d
1wk
4wk
E
DCX
normalized intensity [%]
2d
1wk
4wk
F
Tbr2
normalized counts [%]
2wk
Control
Empty Capsid
G
1µL Saline
1µL 3E12 AAV1-CAG-flex-eGFP
BrdU
3 days
12h
18h
Dapi Casp3
BrdU
H
BrdU
Saline
Virus
normalized counts [%]
12hr
18hr
I
Tbr2
normalized counts [%]
12hr
18hr
J
BrdU & Pyknosis
Average BrdU+ pyknotic cells / section
12hr

7.5%, p=0.003; treatment: n.s., **Fig. 2.2H**), whereas the number of Tbr2+ cells was only decreased 18 hours post injection (treatment: -28.3 ± 6.961, p=0.001; interaction: p=0.09; **Fig. 2.2I**). Cell loss was preceded by an increased number of Caspase-3+ apoptotic cells relative to saline injected controls at 12 hours (treatment: +100.1% ± 19.21%, p<0.001; interaction: p<0.001; 12h: +188.6% ± 29.8%, p <0.0001; 18h:+11.7% ± 24.3%, n.s.; **Fig. S2.2F**). Therefore we determined 12 hours would be a suitable time point to investigate dying cells, before extensive cell loss had occurred. Condensed and fragmented chromatin (pyknosis and karyorrhexis) was identified, in conjunction with BrdU and Caspase-3 (**Fig. 2.2G, inset**). A modest increase in pyknotic and karyorrhexic cells was identified in rAAV-injected DGs relative to their saline injected contralateral controls (+14.7 ± 6.0 cells/section, p= 0.0581, **Fig. S2.2G**). However, a significant increase in pyknosis is seen in BrdU+ proliferating cells (+2.3 ± 0.7 cells/section, p= 0.019; **Fig. 2.2J**). BrdU+ Caspase-3+ double labeled pyknotic cells were rare (n=4 of 887 cells, all in rAAV injected DG), however pyknotic cells were more likely to show Caspase 3 activation following rAAV injection relative to saline controls (+7.7 ± 1.4 cells/section, p=0.003; **Fig. S2.2H**). Taken together this suggests that rAAV injection increases programed cell death of dividing and recently divided cells in the DG.

To determine the effect of viral attachment and penetration in rAAV-induced toxicity we injected 1µL of an equivalent number of empty AAV viral particles (capsid) in DG (**Fig. S2.2E**). Two weeks post-injection there was no effect on Tbr2+ cells relative to the contralateral control (6.8% ± 24.7%, n.s.; **Fig. 2.2F**). We also found that rAAV-induced toxicity was not Sting mediated (BrdU:-90.2% ± 14.2, p<0.001; Tbr2: -88.7% ± 12.9%, p=0.0002; **Fig. S2.2I**). Additionally, while environmental enrichment was sufficient to increase BrdU+ cells, it was insufficient to overcome rAAV-induced toxicity: both BrdU+ cells (Housing: +34.8% ± 11.8%,

p=0.010; Treatment:-109.7% ± 9.9%, p=<0.0001; Interaction: p=0.008; **Fig. S2.2J**) and Tbr2+ cells (Housing: -7.0 ± 8.0, n.s.; Treatment: 95.4 ± 7.9, p<0.0001; Interaction: n.s.; **Fig. S2.2K**) were fully eliminated, suggesting rAAV-induced cell death is not a proportional effect but absolute.

Both systemic and local inflammation are known to negatively impact adult neurogenesis (Ekdahl et al., 2003; Monje et al., 2003). Thus, we investigated whether rAAV-induced cell loss could be explained by inflammation resulting from rAAV infection. In contrast to the rapid loss of NPCs (**Fig. 2.2**), GFAP intensity in the SGZ and hilus is unaffected at 2 days post-injection, slightly increased at 1 week, and greatly increased at 4 weeks (Interaction: p<0.0001; 2 days: +21.6% ± 8.7%, p=0.066; 1 week:+25.2% ± 8.1%, p=0.018; 4 weeks: +165.5% ± 8.7%, p<0.0001, **Fig. S2.2A,B**). Similarly, Iba1 intensity is not increased until 4 weeks post-injection (Interaction: p<0.0001; 2 days:+18.6% ± 10.3%, p=0.243; 1 week: +9.0% ± 9.7%, p=0.739; 4 weeks: +132.4% ± 10.34%, p<0.0001; **Fig. S2.2 B,C**), and no obvious change in microglial morphology was observed at 2 days or 1 week relative to contralateral control. At 4 weeks, microglia exhibit activated amoeboid morphology. Moreover, 30nL nanoinjections of 5E12 GC/mL AAV1-Syn-NES-jRGECO into DG demonstrates incomplete loss of DCX labeling which faithfully follows the boundaries of transgene expression, where cells microns away are spared **(Fig. 2.2D**). These findings suggest that AAV induced toxicity may be cell autonomous and is not likely mediated by astrocyte- or microglial-activated immune responses, or inflammatory signals and other changes within the niche (Ekdahl et al., 2003).

rAAV toxicity in vitro

To determine if rAAV-mediated toxicity is a cell-autonomous phenomenon, we developed an *in vitro* assay to study rAAV-induced elimination of NPCs . Mouse NPCs were

plated, administered with AAV with a multiplicity of infection (MOI) of 1E4 TO 1E7 or water control, and chronically imaged to examine cell survival and proliferation. Dose-dependent inhibition of NPC proliferation and cell death was seen most strongly in NPCs infected with rAAV 1E7 MOI and to a moderate amount in NPCs infected with 1E6 MOI. Within 24 hours of rAAV application, NPCs infected with 1E7 MOI had ceased to proliferate, whereas application of 1E6 MOI resulted in slower proliferation, and 1E5 &1E4 MOI were not different from H2O control **(Fig. 2.3A,C**). Dying cells, visualized by permeability to propidium iodide, increase most significantly in NPCs infected with 1E7 MOI, with an intermediate increase in cell death in mNPCs infected with 1E6 MOI (**Fig. 2.3B,C**). 1E5 and 1E4 MOI infected NPCs were indistinguishable from H2O control.

We then examined whether the minimal AAV genome required for viral encapsulation, two 145bp ITRs, was sufficient to induce cell death, as previously reported in embryonic cells (Hirsch et al., 2011). NPCs were electroporated with "high" (5E6 copies/cell) and "low" (1E6 copies/cell) doses of 145bp rAAV ITR ssDNA, scrambled control, or water and were plated for imaging (as above) or for FACS analysis (schematic in **Figure3D**). In the high dose ITR condition, mNPCs were significantly decreased by 6 hours post-electroporation (-8.1% ± 2.5%, p=0.005) and had ceased expansion by 40 hours (**Fig. 2.3E**). Low dose ITR and high and low dose scramble were indistinguishable from H20 control. Dying cells increased in all groups in the first 24 hours following electroporation (**Fig. 2.3F**). The proportion of the dying, propidium iodide+, cells decreased as confluence increased. However, this proportion was greatly increased in the high ITR condition relative to H20 control (15h: 5E6 v H20 +24.2% ± 0.6%, $p<0.0001$; 1E6 v H20 +5.5% ± 0.6%; $p<0.0001$). FACS analysis at 12, 24, and 36 hours shows the

Fig. 2.3. rAAV toxicity *in vitro* (A) Dose-dependent inhibition of mouse NPC proliferation by encapsulated rAAV. Initial multiplicity of infection (MOI) of 1E7 viral particles/cell arrests NPC proliferation by 24 hours, MOI of 1E6 results in slower proliferation relative to H_2O control, MOI of 1E5 and lower are comparable to H_2O control. **(B)** Dose-dependent rAAV-induced-death. MOI of 1E7 and 1E6 result in an increased proportion of propidium iodide+ NPCs. **(C)** Representative images showing confluence (brightfield) and propidium iodide penetration (red) into NPCs 12 and 48 hours post-viral transduction for MOI of 1E7, 1E6, and for H_20 control. **(D)** Experimental design for AAV ITR electroporation. NPCs are electroporated with 5E6 or 1E6 copies of 145bp ssDNA AAV ITR or scrambled control per cell and plated for FACS analysis or with propidium iodide for imaging on an Incucyte S3. **(E)** Dose-dependent cell loss. Electroporation of high dose 5E6 copies/cell of ITR is sufficient to result in cell loss within hours of electroporation and arrest of proliferation by 40 hours, high dose of 5E6 copies/cell of scrambled ITR shows slight decrease in confluence relative to H_2O control, doses of 1e6/cell of ITR or scrambled ITR is indistinguishable from H_2O control. **(F)** Electroporation of ITR is sufficient to induce greater levels of cell death at higher concentration of 5E6 copies/cell. **(G)** FACS analysis demonstrates a dose-dependent effect of ITR on replicating mNPCs whereby cells electroporated with 5E6 copies/cell of ITR are more susceptible ITR-induced cell death in S- and G2- phase and thus are more permeable to UVZombie at 12 hours post-electroporation. **(H)** a substantial number of NPCs in G1 are not permeable to UVZombie regardless of treatment. Data are represented as mean ± s.e.m.

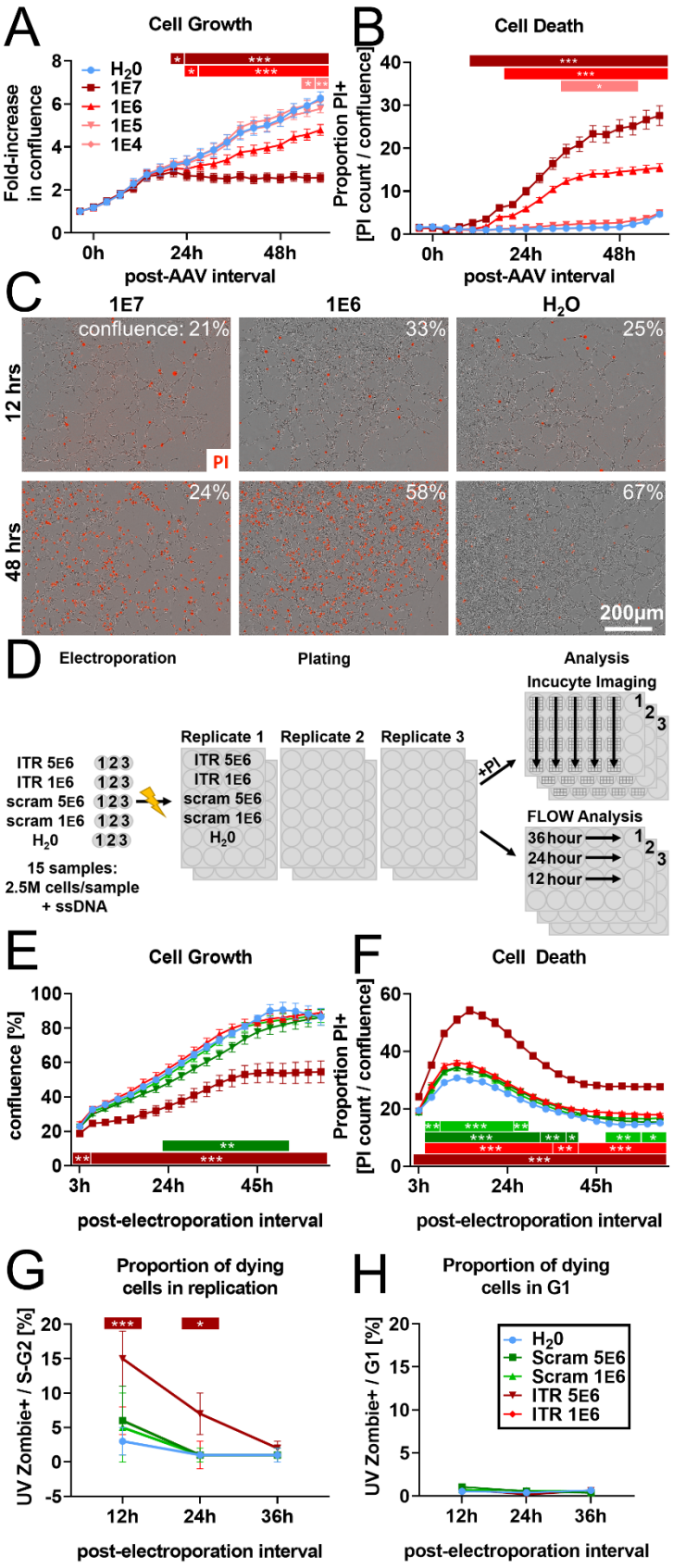
A
Cell Growth
Fold-increase in confluence
H20
1E7
1E6
1E5
1E4
0h
24h
48h
post-AAV interval
B
Cell Death
Proportion PI+ [PI count / confluence]
post-AAV interval
C
1E7
1E6
H2O
confluence: 21%
33%
25%
12 hrs
PI
24%
58%
67%
48 hrs
200µm
D
Electroporation
Plating
Analysis
Incucyte Imaging
ITR 5E6 1 2 3
ITR 1E6 1 2 3
scram 5E6 1 2 3
scram 1E6 1 2 3
H20 1 2 3
15 samples:
2.5M cells/sample
+ ssDNA
Replicate 1
Replicate 2
Replicate 3
ITR 5E6
ITR 1E6
scram 5E6
scram 1E6
H20
+PI
FLOW Analysis
36 hour
24 hour
12 hour
E
Cell Growth
confluence [%]
3h
24h
45h
post-electroporation interval
F
Cell Death
Proportion PI+ [PI count / confluence]
post-electroporation interval
G
Proportion of dying cells in replication
UV Zombie+ / S-G2 [%]
12h
24h
36h
post-electroporation interval
H
Proportion of dying cells in G1
UV Zombie+ / G1 [%]
H20
Scram 5E6
Scram 1E6
ITR 5E6
ITR 1E6
post-electroporation interval

proportion of cells in S/G2 phase that are dying (UVZombie+) is greatly increased at 12 and 24 hours in the high ITR condition, but not in other treatments relative to control (12h: +12.0% ± 2.0%, p <0.0001, **Fig. 2.3G**). The proportion of non-replicating cells that are dying is <1% (**Fig. 2.3H**).

AAV retro serotype permits visualization of dentate granule cells without ablating adult neurogenesis

Given the importance of adult neurogenesis in regulating population activity in the DG, we sought a method that would permit 2-photon calcium imaging of network activity within the DG without ablating neurogenesis. AAV retro is a designer AAV variant, optimized to be taken up by axonal projections (Tervo et al., 2016). We used AAV retro to deliver jRGECO1a to the DG in a retrograde fashion, avoiding infection of immature DGCs whose mossy fiber projections do not reach CA3 until at least 2 weeks of age. Two injections, 400nL each, of AAVretro-CamkIIa::NES-jRGECO1a were made into dorsal CA3 to infect DGCs, and 1µL of either 3E12 AAV1-CAG::flex-eGFP or saline was co-injected into the ipsilateral DG to test the effect of AAV-induced knockdown of neurogenesis.A cranial window to permit 2-photon calcium imaging was implanted to assess the effects of rAAV injection into the DG on DGC activity (schematic in **Fig. 2.4A**). Two weeks after surgery AAV1-CAG::flex-eGFP, but not saline, co-injected animals had reduced adult neurogenesis (BrdU: -41.6% ± 29.3%, p=0.2055, **Fig. 2.4B,C**; DCX -55.6% ± 11.9%, p=0.003, **Fig. 2.4B,D**; Tbr2: -39.2% ± 16.8%, p=0.0806, **Fig. S2.3A,B**). Spontaneous calcium activity was recorded and extracted from these animals from awake implanted mice (**Fig. 2.4E,F; S3C**) and a similar number of active and inactive DGCs was seen across treatment groups (6.9 ± 17.9 cells, n.s. **Fig. 2.4G**). Activity in the DG was decreased in AAV1 injected animals (-135.3 ± 62.4 events/minute, p=0.055, **Fig. 2.4H**). This

Fig. 2.4. AAVretro permits visualization of dentate granule cells without ablating adult neurogenesis (A) Experimental design for 2-photon imaging of DG utilizing AAVretro. 800nL of 3E12 GC/mL AAVretro-Syn-jRGECO and 1μL 3E12 AAV1-CAG-flex-eGFP or Saline are injected into CA3 and DG, respectively. Mice are implanted with a cranial window and undergo 2-photon calcium imaging 2 weeks later. (B) Representative images show BrdU+ and DCX+ cells are intact in animals injected with AAVretro in CA3 when saline is injected into DG but not when AAV1 is injected into DG. **(C)** Quantification of BrdU+ cell survival. Adult neurogenesis is intact in saline co-injected animals, knockdown of adult neurogenesis is variable in AAV1 co-injected animals. **(D)** Quantification of DCX staining demonstrates adult neurogenesis is intact in saline co-injected animals and not intact in AAV1 co-injected animals. This finding is supported by the loss of Tbr2+ intermediate progenitors in AAV1, but not saline, co-injected animals (Fig. S2.3A,B). **(E)** Representative maximum projection image for 2-photon calcium imaging showing cytoplasmic expression of jRGECO in >200 DGCs within a field of view. **(F)** Representative calcium traces of 10 randomly selected neurons from the same animal shown above. **(G)** Total number of identified DGCs in each animal is not-different between saline and AAV1 injected treatment groups. **(H)** AAV1 co-injected animals have fewer total spontaneous calcium transients 2-weeks after injection than saline co-injected controls. **(I)** AAV1 co-injected animals have fewer active cells than saline co-injected controls, and **(J)** though these active cells are not significantly more active (also see Fig. S2.3D,E). Data are represented as mean ± s.e.m.

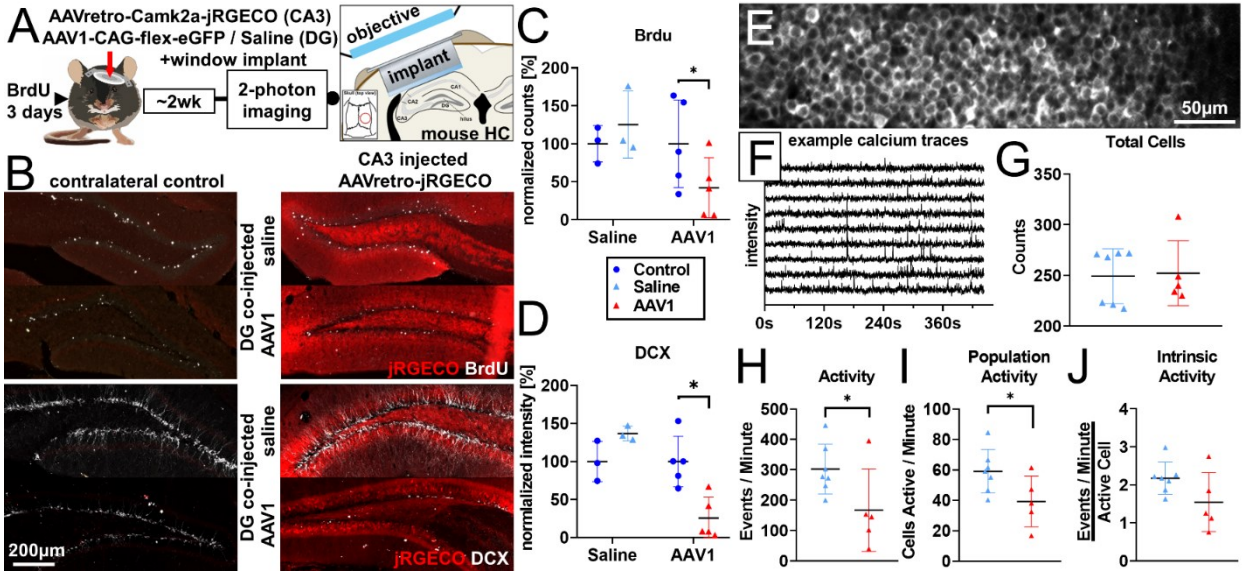
A
AAVretro-Camk2a-jRGECO (CA3)
AAV1-CAG-flex-eGFP / Saline (DG)
+window implant
BrdU
3 days
~2wk
2-photon
imaging
objective
implant
mouse HC
B
contralateral control
CA3 injected
AAVretro-jRGECO
DG co-injected saline
DG co-injected AAV1
jRGECO BrdU
jRGECO DCX
200µm
C
Brdu
normalized counts [%]
Saline
AAV1
Control
Saline
AAV1
D
DCX
normalized intensity [%]
E
50µm
F
example calcium traces
intensity
0s
120s
240s
360s
G
Total Cells
Counts
H
Activity
Events / Minute
I
Population Activity
Cells Active / Minute
J
Intrinsic Activity
Events / Minute
Active Cell

was reflected in a decrease in the average number of active cells per minute (-19.9 ± 9.0 active cells/minute, p=0.05, **Fig. 2.4I, S2D**) but not to the same degree in the firing rate of individual active cells (-0.6 ± 0.3 events/minute/cell, p=0.098; **Fig. 2.4J, S2E**). The size of the calcium transients, measured by amplitude (**Fig. S2.2F,G**) or area under the curve (**Fig. S2.2H**), were not different between treatments. This suggests that the elimination of 2-3 weeks old abDGCs modulates activity in the DG by changing the number of mature DGCs which contribute to DG activity, without drastically changing the firing properties of individual DGCs.

DISCUSSION

Sensitivity of dividing NPCs to rAAV

Based on stable transgene expression in post-mitotic cells, low risk of insertional mutagenesis, and diminished immunogenicity, AAV has seen widespread use as a genetic tool for the visualization and manipulation of cellular processes *in vivo* (Samulski and Muzyczka, 2014). Current recombinant AAV (rAAV) technology allows for the production of replication incompetent viral vectors, with only two 145bp ITRs as the sole viral sequences supplied with the transgene *in cis.* Further development and engineering of new AAV capsids has permitted tissue and cell-type specific expression. Most exciting has been the proposal of rAAV for gene therapy in which a corrective gene is expressed by direct injection of the virus into a tissue of choice (Bartus et al., 2013; Christine et al., 2009; Mandel, 2010) or injected systemically (Bevan et al., 2011; Bryant et al., 2013; Deverman et al., 2016; Foust et al., 2009; Mendell et al., 2017) to compensate for genetic dysfunction and ameliorate disease phenotypes (Büning and Schmidt, 2015).

Despite high rates of infection among humans (Thwaite et al., 2015), AAV infection has not been associated with illness or pathology (Büning and Schmidt, 2015). More than 100

clinical trials using AAV vectors have claimed vector safety (Choudhury et al., 2017; Hocquemiller et al., 2016; Hudry and Vandenberghe, 2019), with transient hepatitis as the most severe side effect. Recently, an AAV2 vector (Luxturna) was the first FDA approved *in vivo* gene therapy (Smalley, 2017).

However, recent reports have suggested rAAV may have some intrinsic toxicity. First, AAV is known to preferentially insert into the AAVS1 locus (Kotin et al., 1990; Samulski et al., 1991) in a *rep* dependent fashion. While the majority of preclinical trials have found rare insertions outside the AAVS1 locus, and argue against insertion-induced genotoxicity (Inagaki et al., 2007; Kaeppel et al., 2013; Nakai et al., 2003, 2005; Nault et al., 2015; Pañeda et al., 2013), several studies have linked insertions of rAAV in open-chromatin to genotoxicity in the liver and hepatocellular carcinoma (Chandler et al., 2015; Donsante et al., 2007; Nault et al., 2015; Rosas et al., 2012). Second, Hirsch et al. (Hirsch et al., 2011) demonstrated rapid induction of cell-death in human embryonic stem cells following rAAV transduction, in which AAV2 ITRs are sufficient to induce death in a p53-dependent manner, independent of *rep*. Third, recent reports from Wilson and colleagues have found severe toxicity in multiple tissue types following systemic injection of rAAV and extended support for claims of hepatotoxicity in NHPs (Hinderer et al., 2018; Hordeaux et al., 2018). These reports further demonstrated sensory and motor neuron degeneration in the dorsal root ganglia and spinal cord of piglets and NHPs, with measurable sensory-motor behavioral deficits in piglets 14 days after systemic injection of AAV9, requiring premature euthanasia (Flotte and Büning, 2018; Hinderer et al., 2018). This toxicity is independent of viral serotype, promoter, and transgene expression; but dependent on viral genome packaging and titer, suggesting an intrinsic mechanism for toxicity of AAV in some cell types.

We have demonstrated dose-dependent rAAV-induced ablation of abDGCs up to 1 week of age in the dentate gyrus (**Fig. 2.1**). Doses used to ablate abDGCs are within and below the range of experimentally relevant titers commonly used for hippocampus research (Anacker et al., 2018; Castle et al., 2018; Danielson et al., 2016, 2017; Gong and Zhou, 2018; Hashimotodani et al., 2017; Hayashi et al., 2017; Kaspar et al., 2002; Kirschen et al., 2017; Liu et al., 2012; McAvoy et al., 2016; Ni et al., 2019; Pilz et al., 2016; Ramirez et al., 2013; Raza et al., 2017; Redondo et al., 2014; Senzai and Buzsáki, 2017; Swiech et al., 2015; Zetsche et al., 2017). rAAV-induced cell-death is rapid and persistent. BrdU-labeled cells and Tbr2+ intermediate progenitors begin to die by 12 and 18 hours post-injection, are almost completely eliminated by 48 hours, and do not recover (**Fig. 2.2B-J**). The initial loss of Tbr2+ intermediate progenitors appears to drive the progressive loss of DCX labeled immature neurons, with no evidence of recovery when assessed at 3 months post-injection (**Fig. S2.2L**). Interestingly, largely quiescent Sox2+ NPCs do not appear equally affected, particularly after 1 week (**Fig. 2.2 B,C**).

In vitro application of rAAV or electroporation of AAV2 ITRs is sufficient to induce arrest of proliferation and cell death (**Fig. 2.3**). This is consistent with the finding that rAAV-induced toxicity the peak in inflammation is not commensurate with (**Fig. S2.2A-D**), is independent of transgene expression and capsid exposure (**Fig. S2.1A, 2F**), and cell-autonomous (**Fig. S2.2D**). Analysis with FACS demonstrates that the high ITR dose results in a disproportionate loss of dividing cells (**Fig. 2.2G,H**). Taken with the above, this suggests the transition from quiescent, slowly dividing Sox2+ Type 1 progenitors to faster dividing Tbr2+ Type 2 progenitors represents a critical junction. The persistence of Sox2 expression in dividing Type 2a progenitors may account for the initial modest decrease seen in Sox2+ cells (Gonçalves et al., 2016a; Kempermann et al., 2015). The preservation of Type 1 progenitors therefore may

not be inconsistent with the findings of (Song et al., 2012) who were able to visualize GABA induced Nestin-GFP+ radial glial cell proliferation even in the presence of AAV titers greater than those reported here.

Dividing cells are implicated in previous reports of AAV-induced toxicity, which were also shown to be independent of immune response to capsid or transgene expression (Hinderer et al., 2018; Hirsch et al., 2011; Hordeaux et al., 2018). Reported liver toxicity is likely derived from increased viral load due to the liver selective tropism of AAV9 (Pulicherla et al., 2011). AAV4 has been similarly described as targeted to quiescent neural stem cells in the DG at low titers, but more widely infective at higher titers (Crowther et al., 2018), suggesting a preferential tropism for stem cells in the DG. Schaffer and colleagues labeled progenitors in the DG and SVZ at relevant titers using other AAV serotypes (Kotterman et al., 2015; Ojala et al., 2018), however the effect of cell-loss was not investigated. Neural progenitor sensitivity may be similarly derived from a broader sensitivity to viral infection (Li et al., 2016; Nowakowski et al., 2016; Tang et al., 2016) and taken together with the above might provide deeper insights into stem cell biology.

2-week old abDGCS contribute to DG activity

Through *in vivo* electrophysiological recordings and optogenetic silencing, the activity of dentate granule cells has been associated with hippocampus-dependent behavioral pattern separation and pattern completion (Danielson et al., 2016; Leutgeb et al., 2007; Nakashiba et al., 2012; Neunuebel and Knierim, 2012). Further, DG computation appears to depend on the addition of abDGCs (Clelland et al., 2009; Ikrar et al., 2013; Sahay et al., 2011). The contribution of abDGCs to DG activity has traditionally focused on cells 4-6 weeks of age, while these cells undergo a critical period of hyper-excitability and enhanced plasticity, after the

formation of mossy fiber terminals in CA3. As described above, *in vivo* optical methods have provided access to study heterogenous and rare populations of cells within the DG (Anacker et al., 2018; Danielson et al., 2016, 2017; Gonçalves et al., 2016b; GoodSmith et al., 2017; Hayashi et al., 2017; Kirschen et al., 2017; Nakazawa, 2017; Pilz et al., 2016, 2018; Senzai and Buzsáki, 2017). However, in studies in which rAAV was injected into DG, neurogenesis was not assessed following viral transduction. Danielson et al. 2016 reported *in* vivo calcium imaging of adult-born and mature DGCs using rAAV for delivery of Gcamp6. In this paradigm abDGCs were labeled with Tamoxifen in a Nestin-CreER x tdTomato reporter mouse 3 weeks before rAAV injection. Imaging took place 3 weeks later, when tdTomato labeled cells would have been ~6 weeks of age, but ongoing neurogenesis was not assessed. This paradigm would permit tdTomato labeled abDGCs 3 weeks of age at rAAV injection, and 6 weeks old at imaging, to largely escape rAAV-induced toxicity. However the loss of abDGCs ~4 weeks old and younger, and their contribution to activity in the DG, might be missed. The methods for AAVretro injection to CA3 described here provide an important advance for future studies of the DG, as granule cells can now be imaged with adult neurogenesis intact.

While abDGCs are believed to be electrophysiologically "silent" up to 1 week of age, they begin receiving functional excitatory GABAergic inputs at 1 week of age and excitatory glutamatergic inputs by 2 weeks of age (Espósito et al., 2005; Ge et al., 2006). These cells, younger than 4 weeks of age, are presumed to play a role modulating DG activity through feedback inhibition and excitation from the hilus, as synapses are formed *en passent* onto hilar interneurons by 1 and 2 weeks post-mitosis (Gu et al., 2012; Ide et al., 2008; Restivo et al., 2015; Toni et al., 2008). These synapses are stably formed by 2 weeks and do not appear to change at

later time points. However, these synapses have not been functionally tested; even the exact contribution of abDGCs at 4-weeks old remains unknown.

Despite a variety of literature on the role of 4-6 week old abDGCs and explicit behavioral evidence that silencing this population of cells at 4 weeks of age disrupts memory retrieval in (Gu et al., 2012), electrophysiological recordings failed to strongly recruit feedback onto the DG at 4 weeks (Temprana et al., 2015), and the same behavioral report failed to find an effect of silencing abDGCs at 2 weeks of age(Gu et al., 2012). Given that these synapses do not appear to change after 2 weeks, if this weak feedback is sufficient to affect DG activity at 4 weeks of age then presumably abDGCs play a role in modulating DG activity at 2 weeks of age. Findings in this paper offer first evidence that 2-3 week old abDGCs cells play a role maintaining the tone of DG activity before strong direct connections to CA3 are established (**Fig. 2.4, S3**). The loss of these cells results in a decrease in mature DG activity.

Caveats for Gene Therapy

rAAV technologies offer tremendous hope for treating a variety of genetically derived illnesses. Systemically injected rAAVs are unlikely to reach the MOI described above that result in rAAV-induced toxicity. However, our results identify particular cases that require added caution. First, high titers may still be achieved in studies injected intrathecally or directly into brain tissue (Bartus et al., 2013; Castle et al., 2018; Christine et al., 2009; Hammond et al., 2017; Mandel, 2010; Nagahara et al., 2013; Tuszynski et al., 2015). Second, while the preferential targeting of current systemically injected rAAVs to neurons and astrocytes permit reduced viral load in off-target tissues (Bevan et al., 2011; Deverman et al., 2016; Foust et al., 2009) it is important to remember MOI calculations in these preferentially targeted tissues might not be straightforward without detailed examination, particularly if stem biology is particularly

susceptible to viral infection. We also demonstrate the late contribution of inflammation, not commensurate with earlier cell loss. The relative costs and benefits of these systems should be weighed where significant gain of life might be conferred (Mendell et al., 2017).

METHODS

Animal use

All animal procedures were approved by the Institutional Animal Care and Use Committees of the Salk Institute and the University of California San Diego, and all experiments were conducted according to the US Public Health Service guidelines for animal research. Wild-type male C57BL/6J mice (Jackson Laboratories), 6 to 7 weeks of age at the time of surgery, were used in this study. Unless otherwise noted, mice were group housed with up to 5 mice per cage in regular cages (RC; 4.7" L × 9.2" W × 5.5" H, InnoVive, San Diego, CA) under standard conditions, on a 12h light–dark cycle, with *ad libitum* access to food and water. BrdU (Sigma) was administered i.p. at 50mg/kg/day for 3 days.

Viral injection

Mice were anesthetized with isoflurane (2% via a nose cone, vol/vol), administered with dexamethasone (2.5 mg/kg, i.p.) to decrease inflammation, and placed in a stereotaxic frame. One microliter of virus solution diluted in sterile saline or saline control, unless otherwise specified, was delivered to the hippocampus through stereotaxic surgery using a microinjector (Nanoject III, Drummond Science). Specifically, the difference between bregma and lambda in anteroposterior coordinates was determined. From bregma, DG injection coordinates were calculated as follows:

Table 1. DG Injection coordinates Injection coordinates as measured from bregma adjusted for measured distance between lambda & bregma (Λ-B): anterior-posterior (A/P), medial-lateral (M/L); and dorsoventral depth from dura (D/V).

Λ-B [mm]	A/P [mm]	M/L [mm]	D/V [mm]
3.0	-1.5	±1.5	-1.8
3.2	-1.6	±1.55	-1.8
3.4	-1.7	±1.6	-1.9
3.6	-1.8	±1.65	-1.9
3.8	-1.9	±1.7	-1.95
4.0	-2.0	±1.75	-2.0

, CA3 injection coordinates were calculated as follows: anteroposterior (A/P) -1.8mm, lateral (M/L) -1.8mm, ventral (V/L; from dura) -1.6mm & -1.8-2.0mm, with 400nL injected at each stop. Following completion of the surgery, carprofen (5 mg/kg, i.p.) and buprenorphine (0.1 mg/kg, s.c.) were administered for inflammation and analgesic relief. Mice were allowed to recover and then returned to their cages. The following viral vectors were used: AAV1-CAG::flex-eGFP-WPRE-bGH (Zeng – Addgene Plasmid #51502, U Penn Vector Core & Addgene), AAVretro-CaMKIIa::NES-jRGECO1a-WPRE-SV40 (Gage, Salk), AAV8-CaMKIIa::NES-jRGECO1a-WPRE-SV40 (Gage, Salk), AAV1-Syn::NES-jRGECO1a-WPRE-SV40 (Kim – Addgene Plasmid# 100854, U Penn), AAV8-CaMKiia::mCherry-WPRE-bGH (Deisseroth – Addgene Plasmid #114469, Salk), AAV8 capsid (Salk).

Enriched/Novel environments

Mice assigned to enriched environments (EE) were housed in regular caging (RC) then moved to an EE cage while matched RC controls remained in RC. The EE cage (36” L × 36” W × 12” H) contained a feeder, 2-3 water dispensers, a large and a small running wheel and multiple plastic tubes and domes, paper huts, on a 12h light–dark cycle. Objects in the EE cage were kept constant throughout the experiment, placement of the objects was altered only to the extent that the mice moved them within the cages. Mice were kept in EE or RC for 13 days and injected with BrdU on the final three days. On the final day of BrdU, mice were also unilaterally injected with 1uL 3E12 GC/mL AAV1-CAG-flexGFP into the DG. Following surgery, animals were returned to EE or RC and sacrificed 2 days post-injection. Mice that received Novel Environment (NE) exposure for cFOS activation experiments remained in RC until NE exposure and were then transferred to EE cages (as described above) for 15-minutes. Animals were sacrificed and tissue collected 1 hour later.

Cranial window placement

For 2-photon calcium imaging experiments, ~1 hour after receiving viral injections as described above, a ~3 mm diameter craniotomy was performed, centered around the DG viral injection site. The underlying dura mater was removed and the cortex and corpus callosum were aspirated with a blunt tip needle attached to a vacuum line. Sterile saline was used to irrigate the lesion and keep it free of blood throughout the surgery. A 3-mm diameter, 1.4-mm deep titanium window implant with a glass coverslip bottom was placed on the alveus of the hippocampus. The implant was held in place with dental cement. A small titanium headbar was attached to the skull to secure the animal to the microscope stage. Following completion of the surgery, carprofen (5 mg/kg, i.p.) and buprenorphine (0.1 mg/kg, s.c.) were administered (as previously mentioned,

animals only received 1 dose of each at the end of the final surgery) for inflammation and analgesic relief. Mice were allowed to recover and then returned to their cages. We have previously found surgical implant and imaging procedures do not affect adult neurogenesis (please see Gonçalves et al. 2016, Fig. S2.8 & S9).

Two-photon calcium imaging of DG activity

Mice were acclimated to head-fixation beginning 1 week after surgery. At time of imaging, each mouse was secured to a goniometer-mounted head-fixation apparatus and a custom-built interferometer was used to level the plane of the cranial window coverslip perpendicular to the imaging path of the microscope objective. Imaging of dorsal DG was performed with a two-photon laser scanning microscope (MOM, Sutter Instruments) using a 1070nm femtosecond-pulsed laser (Fidelity 2, Coherent) and a 16× water immersion objective (0.8 NA, Nikon). Images were acquired using the ScanImage software implemented in MATLAB (MathWorks). Imaging sessions were performed intermittently from 10-18dpi to determine optimal viral expression and imaging window. Analyzed activity videos were acquired at ~14dpi in successive 5-minute intervals (512 x 128 pixels; ~3.91Hz).

Analysis and quantification of calcium activity

Custom software was written in Matlab to extract neuronal activity from 2-photon calcium imaging videos. Calcium traces were extracted by first performing image stabilization for each video using a rigid alignment between frames to maximize the correlation coefficient between frames. Distortion and wobble effects were then corrected using a line-by-line alignment, with distortion prediction informed by the mouse's running data. Automated cell segmentation was then achieved by scanning a ring shape of variable thickness and size across a

motion corrected reference image. When the correlation metric exceeds a user-adjustable threshold, a ring shaped ROI is generated and the signal extracted. User input was then taken for each video to remove false positives and label cells that evaded automatic classification. Once each cell is labeled and the intensities are recorded, the delta fluorescence over the baseline fluorescence (%ΔF/F) is calculated and fit to an exponential curve (is this whole video fluorescence?) to eliminate photo-bleaching effects. Spiking activity for each cell is then inferred from by maximum height of recorded spikes relative to the standard deviation of the signal and the shapes of the spikes. Activity metrics are then generated from the calculated cell activity.

Tissue collection

Mice were anesthetized with a lethal dose of ketamine and xylazine (130 mg/kg, 15 mg/kg; i.p.) and perfused transcardially with 0.9% phosphate buffered saline followed by 4% paraformaldehyde (PFA) in 0.1 M phosphate buffer (pH 7.4). Brains were dissected and post-fixed in 4% PFA overnight then equilibrated in 30% sucrose solution.

Immunohistochemistry

Fixed brains were frozen and sectioned coronally on a sliding microtome at 40-µm thickness, spanning the anterior-posterior extent of the hippocampus,, then stored at −20 °C until staining.

Brain sections were blocked with 0.25% Triton X-100 in TBS with 3% horse serum and incubated with primary antibody in blocking buffer 3× overnight at 4°C. Sections were washed and incubated with fluorophore-conjugated secondary antibodies for 2 hr at RT. DAPI was applied in TBS wash for 15 min at RT. Sections were washed and mounted with PVA-Dabco or Immu-Mount mounting media. For BrdU staining, brain sections were washed 3× in TBS for 5

minutes, incubated in 2N HCL in a 37°C water bath for 30min, rinsed with 0.1M Borate buffer for 10min at RT, washed 6× in TBS for five minutes, then the above staining procedure was followed.

Primary antibodies used were: rat αBrdU (OBT0030, Accurate; NB500-169, Novus; AB6326, Abcam), rabbit αcleaved-CASPASE3 (9661, Cell Signaling), goat αCFOS (sc-52-G, Santa Cruz), rabbit αCFOS (226003, Synaptic Systems), goat αDCX (sc-8066, Santa Cruz), guinea pig αDCX(AB2253, Millipore), chicken αGFAP (AB5541, Millipore), chicken αGFP (GFP-1020, Aves Labs), rabbit αPROX1 (ab101851, Abcam), rabbit αSOX2 (2748, Cell Signaling), rabbit αTBR2 (ab183991, Abcam). Secondary antibodies used were: donkey αchicken-AlexaFlour647 (703-605-155), donkey αchicken-AlexaFluor488 (703-545-155), donkey αrat-AlexaFluor647 (712-605-153), donkey αrabbit-Cy5 (711-175-152) , donkey αrabbit-Cy3 (711-165-152), donkey αrabbit-AlexaFluor488 (711-545-152) donkey αguinea pig-AlexaFluor488 (706-545-148), donkey αguinea pig-Cy3 (706-165-148), donkey αguinea pig-AlexaFlour647 (706-175-148), donkey αgoat – AlexaFlour647(705-175-147), donkey αgoat – Cy3 (705-165-147), donkey αgoat AlexaFlour488 (705-545-147) – (Jackson Immuno Research Laboratories).

Histology acquisition and analysis

Images for analysis of neurogenesis and inflammation markers were acquired using a Zeiss laser scanning confocal microscope (LSM 710, LSM 780, or Airyscan 880) using a 20× objective or an Olympus VS-120 virtual slide scanning microscope using a 10× objective. For confocal images, Z-stacks were obtained through the entirety of the dentate granule cell layer, tiles were stitched using Zen software, and images were maximum projected for quantification. Slide scanner images were obtained from a single plane. For markers quantified by cell counts

(BrdU, TBR2, SOX2, CASPASE3), counting was performed manually. For markers quantified by fluorescent intensity (DCX, IBA1, GFAP), a region of interest was drawn in Zen software, and the average intensity over that region was recorded. For DCX, the region of interest included the full dentate granule cell layer and subgranular zone. Background autofluorescence was corrected by recording the intensity of a neighboring region of CA3 or CA1 devoid of DCX+ cells. For IBA1 and GFAP, the region of interest was the subgranular zone and hilus, bounded by the inner edge of the granule cell layer and a line drawn between the endpoints of the two blades. No background correction was performed for inflammation markers due to the relatively complete tiling of glia throughout the hippocampus. For each brain, 2-5 images were quantified per side. A blinded observer quantified all images.

Images for analysis of pyknosis and karyorrhexis were obtained on an Airyscan 880 microscope using a 40× objective. Z-stacks were obtained through the entirety of the dentate granule cell layer, tiles were stitched using Zen software, and each individual slice of the z-stack was examined. Nuclei were considered abnormal if the DAPI channel showed condensed, uniform labeling throughout the nucleus instead of the typical variation in intensity observed in healthy cells or if nuclei appeared to be fragmenting into uniformly-labeled pieces (Cahill 2017, Bayer and Altman). Two blinded observers quantified these images. The first observer began by identifying abnormal nuclei, then examined that subset of cells for the presence of BrdU or CASPASE3. The second observer began by identifying cells expressing BrdU or CASAPSE3, then examined that subset of cells for nuclear abnormalities. Counts were merged by the first observer for final quantification.

AAV empty capsid

rAAV8 empty capsid were synthesized and purified using standard CsCl rAAV production protocols by Salk Viral Core, without the addition of any ITR containing plasmids or sequences.

Electron microscopy quantification was performed at the Salk Institute's Waitt Advanced Biophotonics Center. 3.5 uL of 3% diluted rAAV empty capsid stock or positive control using viral stock of known concentration (AAV1-CAG-flexGFP) was applied to plasma etched carbon film on 200 mesh copper grids (Ted Pella, 01840-F), 4 grids per stock. Samples were washed three times for 5 seconds, stained with 1% Uranyl Acetate for 1 minute, wicked dry with #1 Whatman filter paper, and air dried before TEM exam. For each grid, 4 fields were selected in each of 4 grid squares, for a total of 16 micrographs per grid, 20000x magnification on a Libra 120kV PLUS EF/TEM (Carl Zeiss), 2kx2k CCD camera. A blinded observer quantified all images.

Cell Culture

Mouse NPCs were obtained from embryonic female C57BL/6 mouse hippocampus and cultured as described previously (Toda et al., 2017). NPCs were cultured in DMEM/F-12 supplemented with N2 and B27 (Invitrogen) in the presence of FGF2 (20 ng/ml), EGF (20 ng/ml), laminin (1 μg/ml) and heparin (5 μg/ml), using poly-ornithine/laminin (Sigma)-coated plastic plates. Media was changed every 2 days, and NPCs were passaged with Accutase (StemCell Tech) when plates reached confluence.

in vitro rAAV transduction imaging

NPCs were seeded onto 96-well plates at a density of 10k cells/well for 24 hours. At 24h media was changed and supplemented with propidium iodide (1μg/mL). To serve as baseline, two sets of images were acquired 4 hours apart in bright field and red-fluorescence: 5 images per well, 8 wells per treatment, for 5 treatments, on an IncuCyte S3 Live Cell Analysis System (Essen Biosciences, Salk Stem Cell Core and UCSD Human Embryonic Stem Cell Core). AAV1-CAG-flex-eGFP was added with an initial MOI at 1E7, 1E6, 1E5, 1E4, or H20 control. MOIs are calculated by dividing total viral particles added per well (1E12, 1E11, 1E10, & 1E9 viral particles, respectively) divided by the initial seeding density of 10k cells/well – this estimate for MOI overestimates the number of viral genomes per cell for two reasons. First, cells were allowed to proliferate for 28h (approximately a 2-3× increase in cells, Fig. 2.3B) before adding virus. Second, viral particles are distributed throughout the growth media and rely on stochastic diffusion for attachment and viral entry into the cells. Images were then acquired every 4 hours for 60 hours. Data was extracted using IncuCyte Analysis software.

In vitro ITR electroporation imaging and FACS analysis

NPCs were collected in nucleofection solution (Amaxa Mouse NSC Nucleofector Kit, Lonza) and electroporated with 5E6 or 1E6 copies/cell of 5’ biotinylated 145bp AAV ITR ssDNA or scrambled control (ITR: 5’-Biotin- AGGAACCCCTAGTGATGGAGTTGGCCACTC CCTCTCTGCGCGCTCGCTCGCTCACTGAGGCCGGGCGACCAAAGGTCGCCCGACGCC CGGGCTTTGCCCGGGCGGCCTCAGTGAGCGAGCGAGCGCGCAGAGAGGGAGTGGCC AA-3’, scramble: 5’-Biotin-CCACATACCGTCTAACGTACGGATTCCGATGCCCAGATAT ATAGTAGATGTCTTATTTGTGGCGGAATAGCGCCAGAGCGTGTAGGCCAACCTTAGT

TCTCCATGGAAGGCATCTACCGAACTCGGTTGCGCGGCCAAATTGGAT-3', Integrated DNA technologies) or with H20, in triplicate, then plated onto 24-well plates (see schematic in **Fig. 2.3D**). AAV2 ITR sequences were obtained from NCBI Viral Genome database, NC_001401.2 (Brister et al., 2015). AAV2 ITRs or a sequence largely homologous with the AAV2 ITR sequence, are used in the vast majority of rAAV plasmids. 24-well plates were segregated for imaging and FACS experiments. Imaging plates were supplemented with propidium iodide and images were acquired on an IncuCyte S3 Live Cell Analysis System as follows: 16 images per well, 4 wells per replicate, 3 replicates per treatment, for 5 treatments, every 3 hours for 60 hours. Data was extracted using Incucyte Analysis software using the same mask definition obtained above. NPCs from FACS plates were collected in PBS at 12, 24, and 36 hours using Accutase. After incubation for 30 minutes at RT with Vybrant DyeCycle Green Stain (ThermoFischer, 1:2000), Zombie UV Fixable Viability Kit (BioLegend, 1:1000) and CountBright Absolute Counting Beads (~5000 beads/sample, Thermofisher), cells were filtered into polypropylene FACS collection tubes and FACS analysis was performed on an LSRFortessa X-20 (BD Biosciences, UCSD Human Embryonic Stem Cell Core). Samples were collected by gating on 1000 CountBright Counting Bead counts per well, 1 well per replicate, 3 replicates per treatment, for the 5 treatments, interleaved, at 3 time points. Populations of live and dead cells (UV Zombie negative and positive cells, respectively), and G1-phase and replicating (S- & G2-phase) cells (Vybrant DyeCycle Green low and high, respectively) were determined using FlowJo software.

Statistical analysis

All data are presented as mean ± s.e.m. To compare histology data across experiments, counts and intensity measures for the injected side of the DG are presented as a percentage of

that group's mean counts or intensity on the control side. Statistical comparisons were performed in Prism 8.0 (GraphPad Software) using paired t-test (paired data, one independent variable: treatment), repeated measures two-way ANOVA using either the Tukey or Sidak multiple comparison test (two independent variables: treatment and time) or 2-way ANOVA using Dunnett's multiple comparison test (*in vitro* rAAV transduction and ITR electroporation relative to H20 control). Linear Regression was performed for BrdU vs cFOS activation. K-S tests were performed for cumulative distributions. All statistical tests were two-tailed. Threshold for significance (α) was set at 0.05, * is defined as $p<0.05$, ** is defined as $p<0.01$, *** is defined as $p<0.001$, n.s. is not significant.

Acknowledgements

We thank Dr. Matt Hirsch, Dr. Jude Samulski, Dr. Tomo Toda, Dr. Simon Schafer, Dr. Carol Marchetto, Lynne Moore, Ruth Beasley for experimental advice, and Mary Lynn Gage for comments on the manuscript. This work was made possible by our funding sources: NIH R01 MH090258, NIH R01 MH095741 NIH R01 AG056306, NIH K08 NS093130, The McKnight Endowment Fund for Neuroscience, JPB Foundation, Annette Merle-Smith, James S. McDonnell Foundation, Mathers Foundation, the Leona M. and Harry B. Helmsley Charitable Trust grant # 2012-PG-MED002, Ray and Dagmar Dolby Family Fund, Salk Innovation Grant, and the Dan and Martina Lewis Biophotonics Fellows Program. Special thanks to Salk Cores: Waitt Advanced Biophotonics Core, STEM Core, Viral Vector Core supported by Salk Cancer Center, NCI P30 CA014195; and UCSD Human Embryonic Stem Cell Core.

Fig. S2.1. rAAV dependent toxicity (A) rAAV-induced reduction of DCX expression is variable at two weeks post injection, but independent of viral core, purification method, serotype, promoter, and protein expressed. **(B)** Consistent with Fig. 2.1C,D, injected titers of 3E12 result in nearly complete abolition of DCX expression, injected titers of 1E12 GC/mL result in partial abolition of DCX expression, injected titers of 3e11GC/mL result in small loss of DCX expression. **(C)** From Fig. 2.1E, cFOS activation in mature DGCs is significantly correlated with knockdown efficiency of adult neurogenesis.

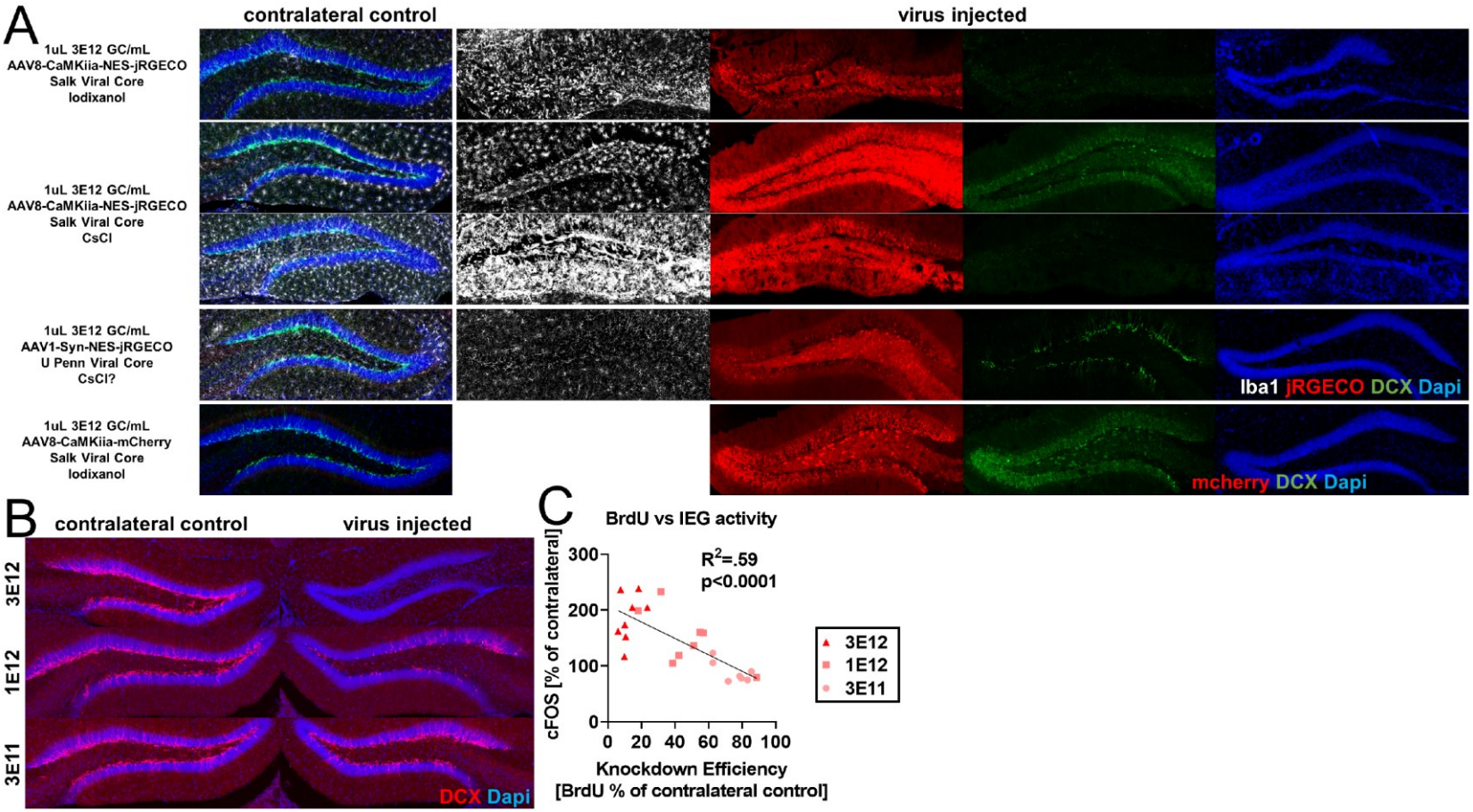
A
contralateral control
virus injected
1uL 3E12 GC/mL
AAV8-CaMKiia-NES-jRGECO
Salk Viral Core
Iodixanol
1uL 3E12 GC/mL
AAV8-CaMKiia-NES-jRGECO
Salk Viral Core
CsCl
1uL 3E12 GC/mL
AAV1-Syn-NES-jRGECO
U Penn Viral Core
CsCl?
Iba1 jRGECO DCX Dapi
1uL 3E12 GC/mL
AAV8-CaMKiia-mCherry
Salk Viral Core
Iodixanol
mcherry DCX Dapi
B
contralateral control
virus injected
3E12
1E12
3E11
DCX Dapi
C
BrdU vs IEG activity
R2=.59
p<0.0001
cFOS [% of contralateral]
300
200
100
0
0 20 40 60 80 100
Knockdown Efficiency
[BrdU % of contralateral control]
3E12
1E12
3E11

Fig. S2.2. Inflammation & cell loss (A) Extending experiments from Fig. 2.2A-E, GFAP intensity is increased in SGZ & hilus 1 week following rAAV injection and greatly increased 4 weeks following injection. **(B)** Iba1 intensity is slightly increased in SGZ & hilus 2 days following rAAV injection and greatly increased 4 weeks following injection. **(C)** Representative images of GFAP and Iba1 histology, increases in GFAP and Iba1 activation are not commensurate with rAAV-induced toxicity. No obvious change in microglial morphology was observed at 2 days or 1 week relative to uninjected contralateral control, at 4 weeks microglia exhibit activated amoeboid morphology. **(D)** Following 30nL injections of 5E12 GC/mL AAV1-Syn-NES-jRGECO, loss of DCX labeling is incomplete and follows boundaries of viral spread. **(E)** Representative image of empty AAV viral particles ("empty capsid") from cryo-electron microscopy used to count effective number of viral particles. **(F)** From Fig. 2.1G, Caspase 3+ cells are increased relative to saline-injected control 12 hours following rAAV injection but match controls at 18 hours. **(G)** Pyknotic and karyorrhexic cells show a non-significant increase in rAAV-injected DG 12 hours post-injection relative to saline control. **(H)** Casp3+ pyknotic cells are significantly increased 12h post-rAAV injection relative to saline controls. **(I)** Injection of 1μL 5E12 GC/mL AAV1-Syn-NES-jRGECO into Sting-KO mice results in BrdU+ and Tbr2+ cell loss. **(J)** Environment enrichment is sufficient to increase adult neurogenesis and increase BrdU labeling, but insufficient to protect against rAAV-induced cell loss. **(K)** Enriched Environment is sufficient to increase Tbr2+ intermediate progenitors, but insufficient to protect against rAAV-induced cell loss**. (L)** Total cells counts using FACS analysis and BrightCount quantification beads show ITR high (5E6 copies/cell) are significantly reduced by 12 hours post electroporation and remain significantly reduced at measured time points. **(M)** Percentage of cells that are replicating at 12 hours is consistently in all groups at 12 hours and 36 hours, but ITR electroporated cells show delay in increasing proliferation and do not represent the same proportion of cells relative to scramble and H_20 electroporated controls.**(N)** Proportion of replicating cells that are dying is increased at 12 hours in ITR electroporated cells but not scramble or H_20 electroporated controls, and return to control levels b 36 hours post-electroporation.

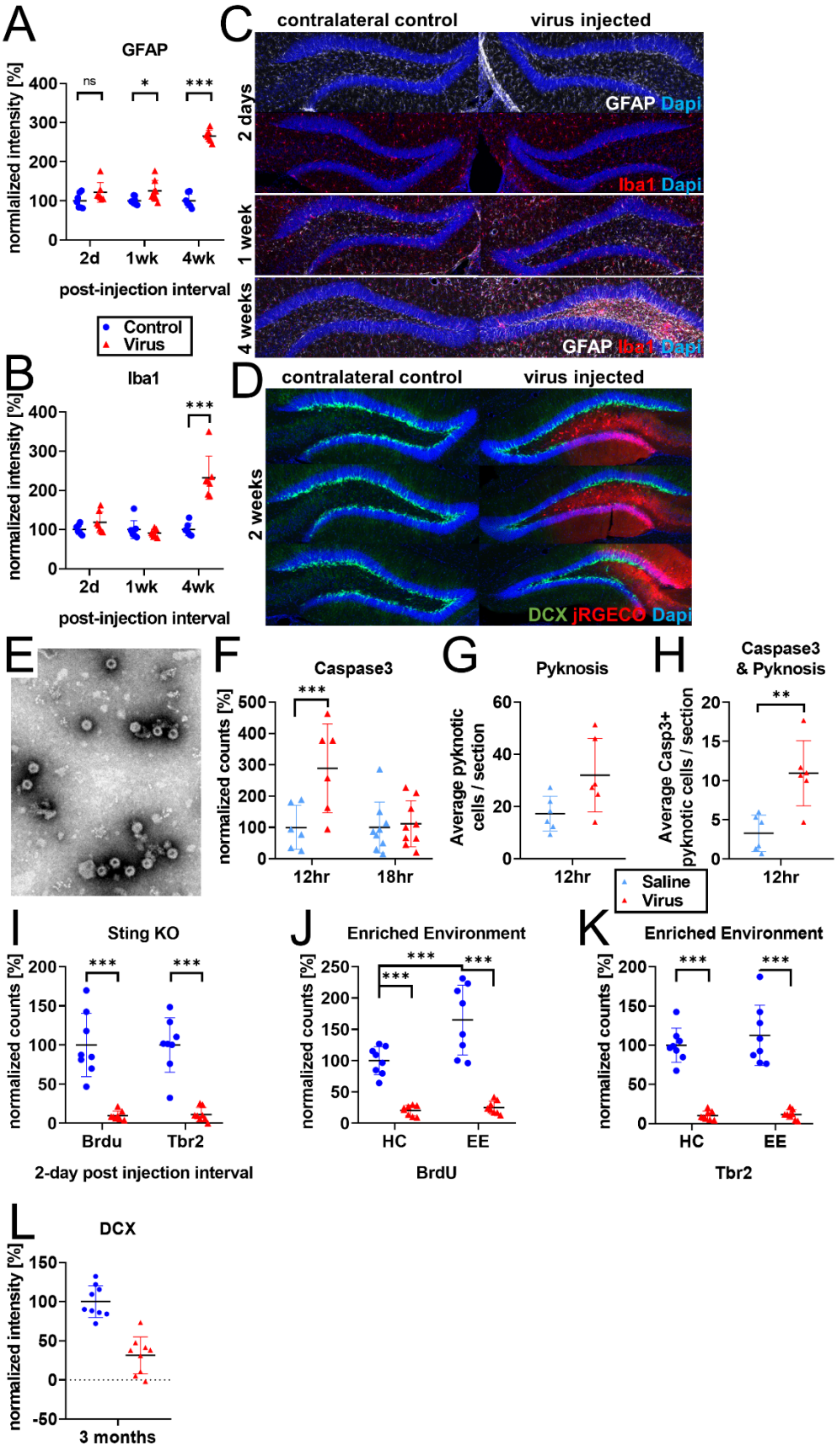
A
GFAP
normalized intensity [%]
ns
*
***
2d
1wk
4wk
post-injection interval
Control
Virus
B
Iba1
normalized intensity [%]
***
2d
1wk
4wk
post-injection interval
C
contralateral control
virus injected
2 days
GFAP Dapi
Iba1 Dapi
1 week
4 weeks
GFAP Iba1 Dapi
D
contralateral control
virus injected
2 weeks
DCX jRGECO Dapi
E
F
Caspase3
normalized counts [%]
***
12hr
18hr
G
Pyknosis
Average pyknotic cells / section
12hr
H
Caspase3 & Pyknosis
Average Casp3+ pyknotic cells / section
**
12hr
Saline
Virus
I
Sting KO
normalized counts [%]
***
***
Brdu
Tbr2
2-day post injection interval
J
Enriched Environment
normalized counts [%]
***
***
***
HC
EE
BrdU
K
Enriched Environment
normalized counts [%]
***
***
HC
EE
Tbr2
L
DCX
normalized intensity [%]
3 months

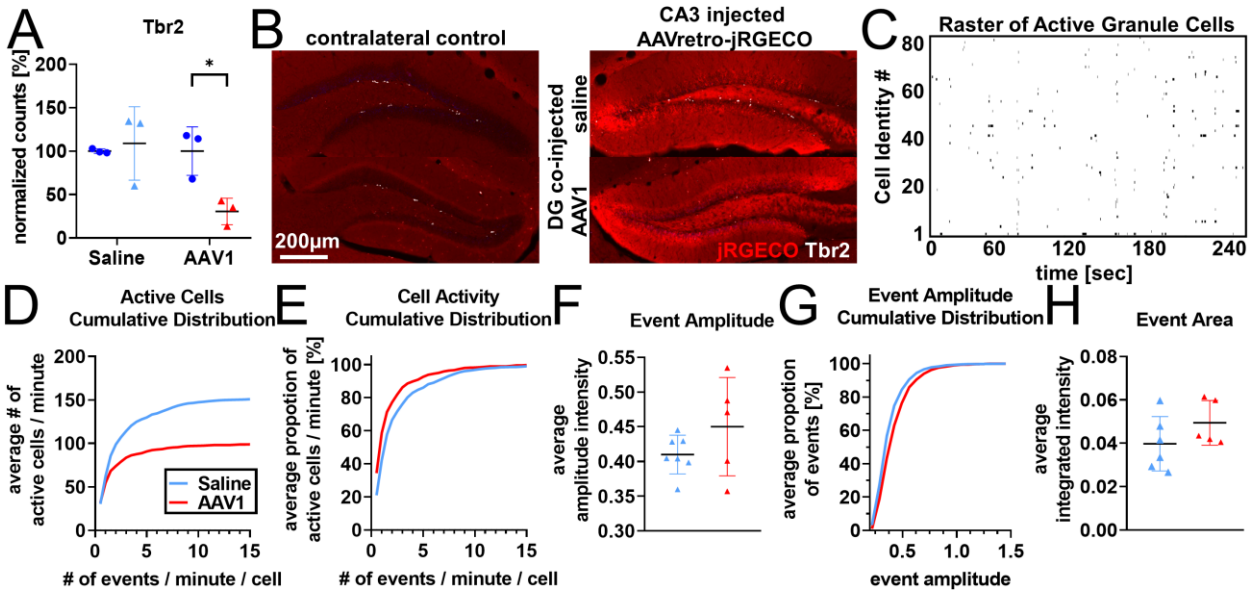

Fig. S3. AAVretro 2-photon calcum imaging (cont'd). **(A)** Consistent with Figure4A-D, Tbr2+ intermediate progenitor cells are intact in saline, but not AAV1, co-injected animals at the time of sacrifice. **(B)** Representative images of Tbr2 staining 2 weeks after co-injection of AAVretro-jRGECO and AAV1 or saline in DG. **(C)** Representative raster plot showing data extracted from calcium imaging transients. **(D)** rAAV co-injected DG have fewer active cells per minute than saline injected animals two weeks post-injection. **(E)** Active DGCs have similar firing rates between rAAV and saline co-injected animals. (**F**) Average event amplitude is not different, and **(G)** the distribution of events amplitudes is not different between saline and rAAV co-injected DGCs. **(H)** Size of events is not different between saline and rAAV conditions. Data are represented as mean ± s.e.m.

REFERENCES

Akers, K.G., Martinez-Canabal, A., Restivo, L., Yiu, A.P., Cristofaro, A.D., Hsiang, H.-L. (Liz), Wheeler, A.L., Guskjolen, A., Niibori, Y., Shoji, H., Ohira, K., Richards, B.A., Miyakawa, T., Josselyn, S.A., and Frankland, P.W. (2014). Hippocampal Neurogenesis Regulates Forgetting During Adulthood and Infancy. Science *344*, 598–602.

Anacker, C., Luna, V.M., Stevens, G.S., Millette, A., Shores, R., Jimenez, J.C., Chen, B., and Hen, R. (2018). Hippocampal neurogenesis confers stress resilience by inhibiting the ventral dentate gyrus. Nature *559*, 98.

Bartus, R.T., Baumann, T.L., Brown, L., Kruegel, B.R., Ostrove, J.M., and Herzog, C.D. (2013). Advancing neurotrophic factors as treatments for age-related neurodegenerative diseases: developing and demonstrating "clinical proof-of-concept" for AAV-neurturin (CERE-120) in Parkinson's disease. Neurobiol. Aging *34*, 35–61.

Bevan, A.K., Duque, S., Foust, K.D., Morales, P.R., Braun, L., Schmelzer, L., Chan, C.M., McCrate, M., Chicoine, L.G., Coley, B.D., Porensky, P.N., Kolb, S.J., Mendell, J.R., Burghes, A.H.M., and Kaspar, B.K. (2011). Systemic gene delivery in large species for targeting spinal cord, brain, and peripheral tissues for pediatric disorders. Mol. Ther. J. Am. Soc. Gene Ther. *19*, 1971–1980.

Brister, J.R., Ako-Adjei, D., Bao, Y., and Blinkova, O. (2015). NCBI viral genomes resource. Nucleic Acids Res. *43*, D571-577.

Bryant, L.M., Christopher, D.M., Giles, A.R., Hinderer, C., Rodriguez, J.L., Smith, J.B., Traxler, E.A., Tycko, J., Wojno, A.P., and Wilson, J.M. (2013). Lessons Learned from the Clinical Development and Market Authorization of Glybera. Hum. Gene Ther. Clin. Dev. *24*, 55–64.

Büning, H., and Schmidt, M. (2015). Adeno-associated Vector Toxicity—To Be or Not to Be? Mol. Ther. *23*, 1673–1675.

Castle, M.J., Cheng, Y., Asokan, A., and Tuszynski, M.H. (2018). Physical positioning markedly enhances brain transduction after intrathecal AAV9 infusion. Sci. Adv. *4*, eaau9859.

Chandler, R.J., LaFave, M.C., Varshney, G.K., Trivedi, N.S., Carrillo-Carrasco, N., Senac, J.S., Wu, W., Hoffmann, V., Elkahloun, A.G., Burgess, S.M., and Venditti, C.P. (2015). Vector design influences hepatic genotoxicity after adeno-associated virus gene therapy. J. Clin. Invest. *125*, 870–880.

Choudhury, S.R., Hudry, E., Maguire, C.A., Sena-Esteves, M., Breakefield, X.O., and Grandi, P. (2017). Viral vectors for therapy of neurologic diseases. Neuropharmacology *120*, 63–80.

Christine, C.W., Starr, P.A., Larson, P.S., Eberling, J.L., Jagust, W.J., Hawkins, R.A., VanBrocklin, H.F., Wright, J.F., Bankiewicz, K.S., and Aminoff, M.J. (2009). Safety and tolerability of putaminal AADC gene therapy for Parkinson disease. Neurology *73*, 1662–1669.

Clelland, C.D., Choi, M., Romberg, C., Clemenson, G.D., Fragniere, A., Tyers, P., Jessberger, S., Saksida, L.M., Barker, R.A., Gage, F.H., and Bussey, T.J. (2009). A Functional Role for Adult Hippocampal Neurogenesis in Spatial Pattern Separation. Science *325*, 210–213.

Clemenson, G.D., Lee, S.W., Deng, W., Barrera, V.R., Iwamoto, K.S., Fanselow, M.S., and Gage, F.H. (2015). Enrichment rescues contextual discrimination deficit associated with immediate shock. Hippocampus *25*, 385–392.

Crowther, A.J., Lim, S.-A., Asrican, B., Albright, B.H., Wooten, J., Yeh, C.-Y., Bao, H., Cerri, D.H., Hu, J., Shih, Y.-Y.I., Asokan, A., and Song, J. (2018). An Adeno-Associated Virus-Based Toolkit for Preferential Targeting and Manipulating Quiescent Neural Stem Cells in the Adult Hippocampus. Stem Cell Rep. *0*.

Danielson, N.B., Kaifosh, P., Zaremba, J.D., Lovett-Barron, M., Tsai, J., Denny, C.A., Balough, E.M., Goldberg, A.R., Drew, L.J., Hen, R., Losonczy, A., and Kheirbek, M.A. (2016). Distinct Contribution of Adult-Born Hippocampal Granule Cells to Context Encoding. Neuron *90*, 101–112.

Danielson, N.B., Turi, G.F., Ladow, M., Chavlis, S., Petrantonakis, P.C., Poirazi, P., and Losonczy, A. (2017). In Vivo Imaging of Dentate Gyrus Mossy Cells in Behaving Mice. Neuron *93*, 552–559.e4.

Deng, W., Saxe, M.D., Gallina, I.S., and Gage, F.H. (2009). Adult-born hippocampal dentate granule cells undergoing maturation modulate learning and memory in the brain. J. Neurosci. Off. J. Soc. Neurosci. *29*, 13532–13542.

Deng, W., Aimone, J.B., and Gage, F.H. (2010). New neurons and new memories: how does adult hippocampal neurogenesis affect learning and memory? Nat. Rev. Neurosci. *11*, 339–350.

Deverman, B.E., Pravdo, P.L., Simpson, B.P., Kumar, S.R., Chan, K.Y., Banerjee, A., Wu, W.-L., Yang, B., Huber, N., Pasca, S.P., and Gradinaru, V. (2016). Cre-dependent selection yields AAV variants for widespread gene transfer to the adult brain. Nat. Biotechnol. *34*, 204–209.

Donsante, A., Miller, D.G., Li, Y., Vogler, C., Brunt, E.M., Russell, D.W., and Sands, M.S. (2007). AAV vector integration sites in mouse hepatocellular carcinoma. Science *317*, 477.

Ekdahl, C.T., Claasen, J.-H., Bonde, S., Kokaia, Z., and Lindvall, O. (2003). Inflammation is detrimental for neurogenesis in adult brain. Proc. Natl. Acad. Sci. *100*, 13632–13637.

Espósito, M.S., Piatti, V.C., Laplagne, D.A., Morgenstern, N.A., Ferrari, C.C., Pitossi, F.J., and Schinder, A.F. (2005). Neuronal Differentiation in the Adult Hippocampus Recapitulates Embryonic Development. J. Neurosci. *25*, 10074–10086.

Flotte, T.R., and Büning, H. (2018). Severe Toxicity in Nonhuman Primates and Piglets with Systemic High-Dose Administration of Adeno-Associated Virus Serotype 9–Like Vectors: Putting Patients First. Hum. Gene Ther. *29*, 283–284.

Foust, K.D., Nurre, E., Montgomery, C.L., Hernandez, A., Chan, C.M., and Kaspar, B.K. (2009). Intravascular AAV9 preferentially targets neonatal-neurons and adult-astrocytes in CNS. Nat. Biotechnol. *27*, 59–65.

Ge, S., Goh, E.L.K., Sailor, K.A., Kitabatake, Y., Ming, G., and Song, H. (2006). GABA regulates synaptic integration of newly generated neurons in the adult brain. Nature *439*, 589.

Gonçalves, J.T., Schafer, S.T., and Gage, F.H. (2016a). Adult Neurogenesis in the Hippocampus: From Stem Cells to Behavior. Cell *167*, 897–914.

Gonçalves, J.T., Bloyd, C.W., Shtrahman, M., Johnston, S.T., Schafer, S.T., Parylak, S.L., Tran, T., Chang, T., and Gage, F.H. (2016b). In vivo imaging of dendritic pruning in dentate granule cells. Nat. Neurosci. *19*, 788–791.

Gong, Z., and Zhou, Q. (2018). Dnmt3a in the dorsal dentate gyrus is a key regulator of fear renewal. Sci. Rep. *8*, 5093.

GoodSmith, D., Chen, X., Wang, C., Kim, S.H., Song, H., Burgalossi, A., Christian, K.M., and Knierim, J.J. (2017). Spatial Representations of Granule Cells and Mossy Cells of the Dentate Gyrus. Neuron *93*, 677–690.e5.

Gu, Y., Arruda-Carvalho, M., Wang, J., Janoschka, S.R., Josselyn, S.A., Frankland, P.W., and Ge, S. (2012). Optical controlling reveals time-dependent roles for adult-born dentate granule cells. Nat. Neurosci. *15*, 1700–1706.

Hammond, S.L., Leek, A.N., Richman, E.H., and Tjalkens, R.B. (2017). Cellular selectivity of AAV serotypes for gene delivery in neurons and astrocytes by neonatal intracerebroventricular injection. PloS One *12*, e0188830.

Hashimotodani, Y., Nasrallah, K., Jensen, K.R., Chávez, A.E., Carrera, D., and Castillo, P.E. (2017). LTP at Hilar Mossy Cell-Dentate Granule Cell Synapses Modulates Dentate Gyrus Output by Increasing Excitation/Inhibition Balance. Neuron *95*, 928–943.e3.

Hayashi, Y., Yawata, S., Funabiki, K., and Hikida, T. (2017). In vivo calcium imaging from dentate granule cells with wide-field fluorescence microscopy. PLOS ONE *12*, e0180452.

Hinderer, C., Katz, N., Buza, E.L., Dyer, C., Goode, T., Bell, P., Richman, L.K., and Wilson, J.M. (2018). Severe Toxicity in Nonhuman Primates and Piglets Following High-Dose Intravenous Administration of an Adeno-Associated Virus Vector Expressing Human SMN. Hum. Gene Ther. *29*, 285–298.

Hirsch, M.L., Fagan, B.M., Dumitru, R., Bower, J.J., Yadav, S., Porteus, M.H., Pevny, L.H., and Samulski, R.J. (2011). Viral single-strand DNA induces p53-dependent apoptosis in human embryonic stem cells. PloS One *6*, e27520.

Hocquemiller, M., Giersch, L., Audrain, M., Parker, S., and Cartier, N. (2016). Adeno-Associated Virus-Based Gene Therapy for CNS Diseases. Hum. Gene Ther. *27*, 478–496.

Hordeaux, J., Wang, Q., Katz, N., Buza, E.L., Bell, P., and Wilson, J.M. (2018). The Neurotropic Properties of AAV-PHP.B Are Limited to C57BL/6J Mice. Mol. Ther. *26*, 664–668.

Hudry, E., and Vandenberghe, L.H. (2019). Therapeutic AAV Gene Transfer to the Nervous System: A Clinical Reality. Neuron *101*, 839–862.

Ide, Y., Fujiyama, F., Okamoto-Furuta, K., Tamamaki, N., Kaneko, T., and Hisatsune, T. (2008). Rapid integration of young newborn dentate gyrus granule cells in the adult hippocampal circuitry. Eur. J. Neurosci. *28*, 2381–2392.

Ikrar, T., Guo, N., He, K., Besnard, A., Levinson, S., Hill, A., Lee, H.-K., Hen, R., Xu, X., and Sahay, A. (2013). Adult neurogenesis modifies excitability of the dentate gyrus. Front. Neural Circuits *7*, 204.

Inagaki, K., Ma, C., Storm, T.A., Kay, M.A., and Nakai, H. (2007). The role of DNA-PKcs and artemis in opening viral DNA hairpin termini in various tissues in mice. J. Virol. *81*, 11304–11321.

Kaeppel, C., Beattie, S.G., Fronza, R., van Logtenstein, R., Salmon, F., Schmidt, S., Wolf, S., Nowrouzi, A., Glimm, H., von Kalle, C., Petry, H., Gaudet, D., and Schmidt, M. (2013). A largely random AAV integration profile after LPLD gene therapy. Nat. Med. *19*, 889–891.

Kaspar, B.K., Vissel, B., Bengoechea, T., Crone, S., Randolph-Moore, L., Muller, R., Brandon, E.P., Schaffer, D., Verma, I.M., Lee, K.-F., Heinemann, S.F., and Gage, F.H. (2002). Adeno-associated virus effectively mediates conditional gene modification in the brain. Proc. Natl. Acad. Sci. U. S. A. *99*, 2320–2325.

Kempermann, G., Song, H., and Gage, F.H. (2015). Neurogenesis in the Adult Hippocampus. Cold Spring Harb. Perspect. Biol. *7*.

Kirschen, G.W., Shen, J., Tian, M., Schroeder, B., Wang, J., Man, G., Wu, S., and Ge, S. (2017). Active Dentate Granule Cells Encode Experience to Promote the Addition of Adult-Born Hippocampal Neurons. J. Neurosci. *37*, 4661–4678.

Ko, H.-G., Jang, D.-J., Son, J., Kwak, C., Choi, J.-H., Ji, Y.-H., Lee, Y.-S., Son, H., and Kaang, B.-K. (2009). Effect of ablated hippocampal neurogenesis on the formation and extinction of contextual fear memory. Mol. Brain *2*, 1.

Kotin, R.M., Siniscalco, M., Samulski, R.J., Zhu, X.D., Hunter, L., Laughlin, C.A., McLaughlin, S., Muzyczka, N., Rocchi, M., and Berns, K.I. (1990). Site-specific integration by adeno-associated virus. Proc. Natl. Acad. Sci. *87*, 2211–2215.

Kotterman, M.A., Chalberg, T.W., and Schaffer, D.V. (2015). Viral Vectors for Gene Therapy: Translational and Clinical Outlook. Annu. Rev. Biomed. Eng. *17*, 63–89.

Lacefield, C.O., Itskov, V., Reardon, T., Hen, R., and Gordon, J.A. (2012). Effects of adult-generated granule cells on coordinated network activity in the dentate gyrus. Hippocampus *22*, 106–116.

Leutgeb, J.K., Leutgeb, S., Moser, M.-B., and Moser, E.I. (2007). Pattern Separation in the Dentate Gyrus and CA3 of the Hippocampus. Science *315*, 961–966.

Li, H., Saucedo-Cuevas, L., Regla-Nava, J.A., Chai, G., Sheets, N., Tang, W., Terskikh, A.V., Shresta, S., and Gleeson, J.G. (2016). Zika Virus Infects Neural Progenitors in the Adult Mouse Brain and Alters Proliferation. Cell Stem Cell *19*, 593–598.

Liu, X., Ramirez, S., Pang, P.T., Puryear, C.B., Govindarajan, A., Deisseroth, K., and Tonegawa, S. (2012). Optogenetic stimulation of a hippocampal engram activates fear memory recall. Nature *484*, 381–385.

Mandel, R.J. (2010). CERE-110, an adeno-associated virus-based gene delivery vector expressing human nerve growth factor for the treatment of Alzheimer's disease. Curr. Opin. Mol. Ther. *12*, 240–247.

McAvoy, K.M., Scobie, K.N., Berger, S., Russo, C., Guo, N., Decharatanachart, P., Vega-Ramirez, H., Miake-Lye, S., Whalen, M., Nelson, M., Bergami, M., Bartsch, D., Hen, R., Berninger, B., and Sahay, A. (2016). Modulating Neuronal Competition Dynamics in the Dentate Gyrus to Rejuvenate Aging Memory Circuits. Neuron *91*, 1356–1373.

Mendell, J.R., Al-Zaidy, S., Shell, R., Arnold, W.D., Rodino-Klapac, L.R., Prior, T.W., Lowes, L., Alfano, L., Berry, K., Church, K., Kissel, J.T., Nagendran, S., L'Italien, J., Sproule, D.M., Wells, C., Cardenas, J.A., Heitzer, M.D., Kaspar, A., Corcoran, S., Braun, L., Likhite, S., Miranda, C., Meyer, K., Foust, K.D., Burghes, A.H.M., and Kaspar, B.K. (2017). Single-Dose Gene-Replacement Therapy for Spinal Muscular Atrophy. N. Engl. J. Med. *377*, 1713–1722.

Monje, M.L., Toda, H., and Palmer, T.D. (2003). Inflammatory Blockade Restores Adult Hippocampal Neurogenesis. Science *302*, 1760–1765.

Nagahara, A.H., Mateling, M., Kovacs, I., Wang, L., Eggert, S., Rockenstein, E., Koo, E.H., Masliah, E., and Tuszynski, M.H. (2013). Early BDNF treatment ameliorates cell loss in the entorhinal cortex of APP transgenic mice. J. Neurosci. Off. J. Soc. Neurosci. *33*, 15596–15602.

Nakai, H., Montini, E., Fuess, S., Storm, T.A., Grompe, M., and Kay, M.A. (2003). AAV serotype 2 vectors preferentially integrate into active genes in mice. Nat. Genet. *34*, 297–302.

Nakai, H., Wu, X., Fuess, S., Storm, T.A., Munroe, D., Montini, E., Burgess, S.M., Grompe, M., and Kay, M.A. (2005). Large-scale molecular characterization of adeno-associated virus vector integration in mouse liver. J. Virol. *79*, 3606–3614.

Nakashiba, T., Cushman, J.D., Pelkey, K.A., Renaudineau, S., Buhl, D.L., McHugh, T.J., Barrera, V.R., Chittajallu, R., Iwamoto, K.S., McBain, C.J., Fanselow, M.S., and Tonegawa, S. (2012). Young Dentate Granule Cells Mediate Pattern Separation, whereas Old Granule Cells Facilitate Pattern Completion. Cell *149*, 188–201.

Nakazawa, K. (2017). Dentate Mossy Cell and Pattern Separation. Neuron *93*, 465–467.

Nault, J.-C., Datta, S., Imbeaud, S., Franconi, A., Mallet, M., Couchy, G., Letouzé, E., Pilati, C., Verret, B., Blanc, J.-F., Balabaud, C., Calderaro, J., Laurent, A., Letexier, M., Bioulac-Sage, P., Calvo, F., and Zucman-Rossi, J. (2015). Recurrent AAV2-related insertional mutagenesis in human hepatocellular carcinomas. Nat. Genet. *47*, 1187–1193.

Neunuebel, J.P., and Knierim, J.J. (2012). Spatial firing correlates of physiologically distinct cell types of the rat dentate gyrus. J. Neurosci. Off. J. Soc. Neurosci. *32*, 3848–3858.

Ni, S., Huang, H., He, D., Chen, H., Wang, C., Zhao, X., Chen, X., Cui, W., Zhou, W., and Zhang, J. (2019). Adeno-associated virus-mediated over-expression of CREB-regulated transcription coactivator 1 in the hippocampal dentate gyrus ameliorates lipopolysaccharide-induced depression-like behaviour in mice. J. Neurochem. *149*, 111–125.

Nowakowski, T.J., Pollen, A.A., Di Lullo, E., Sandoval-Espinosa, C., Bershteyn, M., and Kriegstein, A.R. (2016). Expression Analysis Highlights AXL as a Candidate Zika Virus Entry Receptor in Neural Stem Cells. Cell Stem Cell *18*, 591–596.

Ojala, D.S., Sun, S., Santiago-Ortiz, J.L., Shapiro, M.G., Romero, P.A., and Schaffer, D.V. (2018). In Vivo Selection of a Computationally Designed SCHEMA AAV Library Yields a Novel Variant for Infection of Adult Neural Stem Cells in the SVZ. Mol. Ther. *26*, 304–319.

Pañeda, A., Lopez-Franco, E., Kaeppel, C., Unzu, C., Gil-Royo, A.G., D'Avola, D., Beattie, S.G., Olagüe, C., Ferrero, R., Sampedro, A., Mauleon, I., Hermening, S., Salmon, F., Benito, A., Gavira, J.J., Cornet, M.E., del Mar Municio, M., von Kalle, C., Petry, H., Prieto, J., Schmidt, M., Fontanellas, A., and González-Aseguinolaza, G. (2013). Safety and liver transduction efficacy of rAAV5-cohPBGD in nonhuman primates: a potential therapy for acute intermittent porphyria. Hum. Gene Ther. *24*, 1007–1017.

Pilz, G.-A., Carta, S., Stäuble, A., Ayaz, A., Jessberger, S., and Helmchen, F. (2016). Functional Imaging of Dentate Granule Cells in the Adult Mouse Hippocampus. J. Neurosci. Off. J. Soc. Neurosci. *36*, 7407–7414.

Pilz, G.-A., Bottes, S., Betizeau, M., Jörg, D.J., Carta, S., Simons, B.D., Helmchen, F., and Jessberger, S. (2018). Live imaging of neurogenesis in the adult mouse hippocampus. Science *359*, 658–662.

Pulicherla, N., Shen, S., Yadav, S., Debbink, K., Govindasamy, L., Agbandje-McKenna, M., and Asokan, A. (2011). Engineering Liver-detargeted AAV9 Vectors for Cardiac and Musculoskeletal Gene Transfer. Mol. Ther. *19*, 1070–1078.

Ramirez, S., Liu, X., Lin, P.-A., Suh, J., Pignatelli, M., Redondo, R.L., Ryan, T.J., and Tonegawa, S. (2013). Creating a False Memory in the Hippocampus. Science *341*, 387–391.

Raza, S.A., Albrecht, A., Çalışkan, G., Müller, B., Demiray, Y.E., Ludewig, S., Meis, S., Faber, N., Hartig, R., Schraven, B., Lessmann, V., Schwegler, H., and Stork, O. (2017). HIPP neurons in the dentate gyrus mediate the cholinergic modulation of background context memory salience. Nat. Commun. *8*, 189.

Redondo, R.L., Kim, J., Arons, A.L., Ramirez, S., Liu, X., and Tonegawa, S. (2014). Bidirectional switch of the valence associated with a hippocampal contextual memory engram. Nature *513*, 426–430.

Restivo, L., Niibori, Y., Mercaldo, V., Josselyn, S.A., and Frankland, P.W. (2015). Development of Adult-Generated Cell Connectivity with Excitatory and Inhibitory Cell Populations in the Hippocampus. J. Neurosci. *35*, 10600–10612.

Rosas, L.E., Grieves, J.L., Zaraspe, K., La Perle, K.M., Fu, H., and McCarty, D.M. (2012). Patterns of scAAV vector insertion associated with oncogenic events in a mouse model for genotoxicity. Mol. Ther. J. Am. Soc. Gene Ther. *20*, 2098–2110.

Sahay, A., Scobie, K.N., Hill, A.S., O'Carroll, C.M., Kheirbek, M.A., Burghardt, N.S., Fenton, A.A., Dranovsky, A., and Hen, R. (2011). Increasing adult hippocampal neurogenesis is sufficient to improve pattern separation. Nature *472*, 466–470.

Samulski, R.J., and Muzyczka, N. (2014). AAV-Mediated Gene Therapy for Research and Therapeutic Purposes. Annu. Rev. Virol. *1*, 427–451.

Samulski, R.J., Zhu, X., Xiao, X., Brook, J.D., Housman, D.E., Epstein, N., and Hunter, L.A. (1991). Targeted integration of adeno-associated virus (AAV) into human chromosome 19. EMBO J. *10*, 3941–3950.

Saxe, M.D., Malleret, G., Vronskaya, S., Mendez, I., Garcia, A.D., Sofroniew, M.V., Kandel, E.R., and Hen, R. (2007). Paradoxical influence of hippocampal neurogenesis on working memory. Proc. Natl. Acad. Sci. U. S. A. *104*, 4642–4646.

Senzai, Y., and Buzsáki, G. (2017). Physiological Properties and Behavioral Correlates of Hippocampal Granule Cells and Mossy Cells. Neuron *93*, 691–704.e5.

Singer, B.H., Gamelli, A.E., Fuller, C.L., Temme, S.J., Parent, J.M., and Murphy, G.G. (2011). Compensatory network changes in the dentate gyrus restore long-term potentiation following ablation of neurogenesis in young-adult mice. Proc. Natl. Acad. Sci. U. S. A. *108*, 5437–5442.

Smalley, E. (2017). First AAV gene therapy poised for landmark approval. Nat. Biotechnol. *35*, 998–999.

Snyder, J.S., Glover, L.R., Sanzone, K.M., Kamhi, J.F., and Cameron, H.A. (2009). The effects of exercise and stress on the survival and maturation of adult-generated granule cells. Hippocampus *19*, 898–906.

Song, J., Zhong, C., Bonaguidi, M.A., Sun, G.J., Hsu, D., Gu, Y., Meletis, K., Huang, Z.J., Ge, S., Enikolopov, G., Deisseroth, K., Luscher, B., Christian, K.M., Ming, G., and Song, H. (2012). Neuronal circuitry mechanism regulating adult quiescent neural stem-cell fate decision. Nature *489*, 150–154.

Swiech, L., Heidenreich, M., Banerjee, A., Habib, N., Li, Y., Trombetta, J., Sur, M., and Zhang, F. (2015). In vivo interrogation of gene function in the mammalian brain using CRISPR-Cas9. Nat. Biotechnol. *33*, 102–106.

Tang, H., Hammack, C., Ogden, S.C., Wen, Z., Qian, X., Li, Y., Yao, B., Shin, J., Zhang, F., Lee, E.M., Christian, K.M., Didier, R.A., Jin, P., Song, H., and Ming, G. (2016). Zika Virus Infects Human Cortical Neural Progenitors and Attenuates Their Growth. Cell Stem Cell *18*, 587–590.

Temprana, S.G., Mongiat, L.A., Yang, S.M., Trinchero, M.F., Alvarez, D.D., Kropff, E., Giacomini, D., Beltramone, N., Lanuza, G.M., and Schinder, A.F. (2015). Delayed coupling to feedback inhibition during a critical period for the integration of adult-born granule cells. Neuron *85*, 116–130.

Tervo, D.G.R., Hwang, B.-Y., Viswanathan, S., Gaj, T., Lavzin, M., Ritola, K.D., Lindo, S., Michael, S., Kuleshova, E., Ojala, D., Huang, C.-C., Gerfen, C.R., Schiller, J., Dudman, J.T., Hantman, A.W., Looger, L.L., Schaffer, D.V., and Karpova, A.Y. (2016). A Designer AAV Variant Permits Efficient Retrograde Access to Projection Neurons. Neuron *92*, 372–382.

Thwaite, R., Pagès, G., Chillón, M., and Bosch, A. (2015). AAVrh.10 immunogenicity in mice and humans. Relevance of antibody cross-reactivity in human gene therapy. Gene Ther. *22*, 196–201.

Toda, T., Hsu, J.Y., Linker, S.B., Hu, L., Schafer, S.T., Mertens, J., Jacinto, F.V., Hetzer, M.W., and Gage, F.H. (2017). Nup153 Interacts with Sox2 to Enable Bimodal Gene Regulation and Maintenance of Neural Progenitor Cells. Cell Stem Cell *21*, 618–634.e7.

Toni, N., Laplagne, D.A., Zhao, C., Lombardi, G., Ribak, C.E., Gage, F.H., and Schinder, A.F. (2008). Neurons born in the adult dentate gyrus form functional synapses with target cells. Nat. Neurosci. *11*, 901–907.

Tronel, S., Belnoue, L., Grosjean, N., Revest, J.-M., Piazza, P.-V., Koehl, M., and Abrous, D.N. (2012). Adult-born neurons are necessary for extended contextual discrimination. Hippocampus *22*, 292–298.

Tuszynski, M.H., Yang, J.H., Barba, D., U, H.-S., Bakay, R.A.E., Pay, M.M., Masliah, E., Conner, J.M., Kobalka, P., Roy, S., and Nagahara, A.H. (2015). Nerve Growth Factor Gene Therapy: Activation of Neuronal Responses in Alzheimer Disease. JAMA Neurol. *72*, 1139–1147.

Vivar, C., Peterson, B.D., and van Praag, H. Running rewires the neuronal network of adult-born dentate granule cells. NeuroImage.

Zetsche, B., Heidenreich, M., Mohanraju, P., Fedorova, I., Kneppers, J., DeGennaro, E.M., Winblad, N., Choudhury, S.R., Abudayyeh, O.O., Gootenberg, J.S., Wu, W.Y., Scott, D.A., Severinov, K., van der Oost, J., and Zhang, F. (2017). Multiplex gene editing by CRISPR-Cpf1 using a single crRNA array. Nat. Biotechnol. *35*, 31–34.

Zhu, H., Pleil, K.E., Urban, D.J., Moy, S.S., Kash, T.L., and Roth, B.L. (2014). Chemogenetic Inactivation of Ventral Hippocampal Glutamatergic Neurons Disrupts Consolidation of Contextual Fear Memory. Neuropsychopharmacology *39*, 1880–1892.

Chapter 2, in full, is coauthored unpublished material: Johnston ST, Parylak SL, Kim S, Mac N, Lim CK, Gallina IS, Bloyd CW, Alex Newberry Saavedra CD, Ondřej Novák, Gonçalves JT, Gage FH, Shtrahman M. AAV induced cell-death of Neural Progenitor Cells in the Dentate Gyrus. The dissertation author was the primary investigator and author of this paper.

CONCLUSION

New *in vivo* optical methods have provided access to study the computations which subserve memory formation and recall within the hippocampal dentate gyrus (DG), and activity of dentate granule cells (DGCs) has been associated with hippocampus-dependent behavior. These computations are further subserved by a rare population of immature adult-born dentate granule cells (abDGCs). Crucially, these studies rely almost exclusively on rAAV for transgene delivery.

We have demonstrated that neural progenitor cells (NPCs) and immature DGCs within the adult murine hippocampus are particularly sensitive to rAAV induced cell-death. Cell loss is dose-dependent and nearly complete at experimentally relevant viral titers. rAAV induced cell-death is rapid and persistent, with loss of BrdU labeled cells within 18 hours post-injection and no evidence of recovery of adult neurogenesis when assessed at 3 months post-injection. This rAAV-induced toxicity is intrinsic to the rAAV viral vector and affects the activity of the remaining mature DGCs at 2 and 4 weeks post-injection. This rAAV induced toxicity further extends an emerging body of work which suggests rAAV may be more toxic than previously believed. Stem cells may be particularly sensitive.

However, we additionally introduce a method that permits efficient transduction for the visualization and manipulation of the DG using rAAV2-retro serotyped virus that does not result in the ablation of abDGCs; leaving adult neurogenesis and its effects on hippocampal network activity intact. This method sets the stage for future work which will permit the manipulation and visualization of DGCs *in vivo* and the contribution of DGC activity to hippocampal computation and hippocampus-dependent to be determined.